Title

Galectin-3 Coordinates a Cellular System for Lysosomal Repair and Removal

Journal

Developmental Cell, 52(1)

ISSN

1534-5807

Authors

Jia, Jingyue
Claude-Taupin, Aurore
Gu, Yuexi
et al.

Publication Date

2020

DOI

10.1016/j.devcel.2019.10.025

Peer reviewed

HHS Public Access

Author manuscript

Dev Cell. Author manuscript; available in PMC 2021 January 06.

Published in final edited form as:

Dev Cell. 2020 January 06; 52(1): 69–87.e8. doi:10.1016/j.devcel.2019.10.025.

Galectin-3 coordinates a cellular system for lysosomal repair and removal

Jingyue Jia[1,2], **Aurore Claude-Taupin**[1,2], **Yuexi Gu**[1,2], **Seong Won Choi**[1,2], **Ryan Peters**[1,2], **Bhawana Bissa**[1,2], **Michal H. Mudd**[1,2], **Lee Allers**[1,2], **Sandeep Pallikkuth**[3], **Keith A. Lidke**[3], **Michelle Salemi**[4], **Brett Phinney**[4], **Muriel Mari**[5], **Fulvio Reggiori**[5], **Vojo Deretic**[1,2,6,*]

[1]Autophagy, Inflammation and Metabolic Center of Biochemical Research Excellence. [2]Department of Molecular Genetics and Microbiology, University of New Mexico Health Sciences Center, 915 Camino de Salud, NE, Albuquerque, NM 87131, USA. [3]Department of Physics and Astronomy, University of New Mexico, Albuquerque, NM 87131, USA. [4]Proteomics Core Facility, UC Davis Genome Center, University of California, Davis, CA 95616, USA. [5]Department of Biomedical Sciences & Systems, University of Groningen, University Medical Center Groningen, Groningen, Netherlands. [6]Lead Contact

SUMMARY

Endomembrane damage elicits homeostatic responses including ESCRT-dependent membrane repair and autophagic removal of damaged organelles. Previous studies have suggested that these systems may act separately. Here we show that galectin-3 (Gal3), a β-galactoside binding cytosolic lectin, unifies and coordinates ESCRT and autophagy responses to lysosomal damage. Gal3 and its capacity to recognize damage-exposed glycans were required for efficient recruitment of the ESCRT component ALIX during lysosomal damage. Both Gal3 and ALIX were required for restoration of lysosomal function. Gal3 promoted interactions between ALIX and the downstream ESCRT-III effector CHMP4 during lysosomal repair. At later time points following lysosomal injury, Gal3 controlled autophagic responses. When this failed, as in Gal3 knockout cells, lysosomal replacement program took over through TFEB. Manifestations of this staged response, which includes membrane repair, removal and replacement, were detected in model systems of lysosomal damage inflicted by proteopathic tau and during phagosome parasitism by *Mycobacterium tuberculosis.*

*Correspondence: Vojo Deretic, Ph.D., Department of Molecular Genetics and Microbiology, University of New Mexico Health Sciences Center, 915 Camino de Salud, NE, Albuquerque, NM 87131, U.S.A., (505) 272-3814, vderetic@salud.unm.edu.

AUTHOR CONTRIBUTIONS

Conceptualization: J.J. and V.D.; Formal Analysis: J.J., A.C., Y.G., S.W.C., R.P., L.A., S.P., M.S. and V.D.; Investigation and Validation: J. J., A.C., Y.G., S.W.C., R.P., B.B., L.A., S.P., M.S., B.P., M.M., F.R. and V.D.; Resources: V.D., K.L., F.R.; Data Curation: J.J., S.W.C., R.P., L.A., S.P.; Writing – Original Draft: J.J. and V.D.; Writing – Review & Editing: J.J., M.S., B.P., M.M., F.R. and V.D.; Visualization: J.J., S.P., K.L., and V.D.; Supervision: V.D., B.P., F.R.; Project Administration: V.D.; Funding Acquisition: V.D.

DECLARATION OF INTERESTS

The authors declare no competing interests.

Graphical Abstract

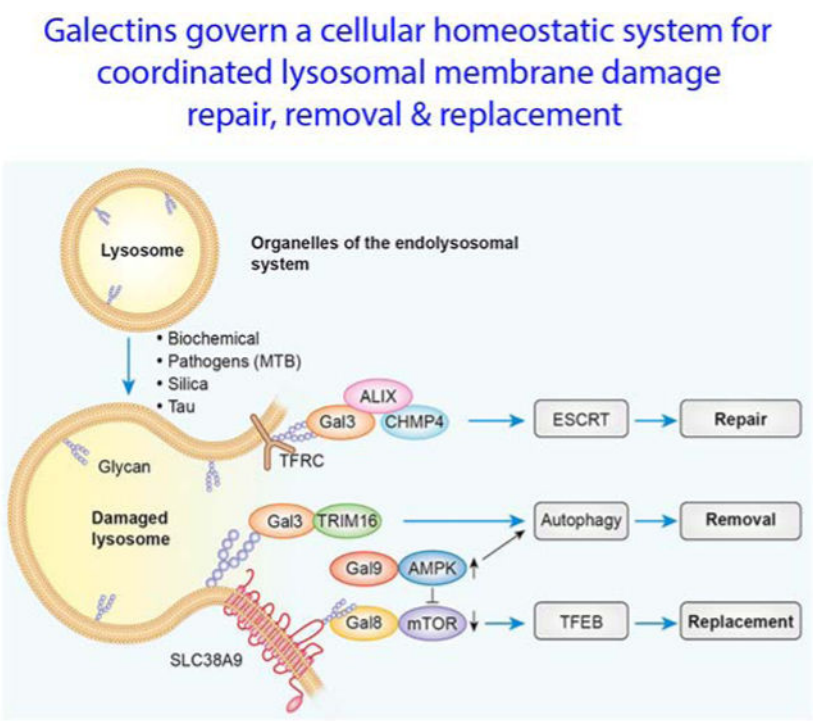

eTOC Blurb

Jia et al., show that Galectin-3 recruits ESCRT components to damaged lysosomes for repair and restoration of their function. During sustained lysosomal injury, galectins induce autophagy and lysosomal biogenesis for a staged repair, removal and replacement program. This response is deployed during damage with neurotoxic tau or *Mycobacterium tuberculosis* infection.

INTRODUCTION

The mammalian cell responds to organellar and plasma membrane damage by deploying a set of activities including those performed by the ESCRT (endosomal sorting complexes required for transport) machinery (Denais et al., 2016; Jimenez et al., 2014; Raab et al., 2016; Radulovic et al., 2018; Scheffer et al., 2014; Skowyra et al., 2018) and autophagy systems (Chauhan et al., 2016; Dupont et al., 2009; Fujita et al., 2013; Thurston et al., 2012; Wei et al., 2017; Yoshida et al., 2017). The contributions of ESCRT (Radulovic et al., 2018; Skowyra et al., 2018) and autophagic responses (Jia et al., 2018; Maejima et al., 2013; Yoshida et al., 2017) during lysosomal membrane damage have received recent attention in the context of maintaining endolysosomal system homeostasis. However, whether and how ESCRT and autophagy cooperate during endomembrane damage is not well understood. Previous studies suggest that these systems may act independently when lysosomes are damaged (Radulovic et al., 2018; Skowyra et al., 2018).

The mechanism for how ESCRT act in membrane repair, including during lysosomal damage, is believed to be membrane scission and closure (Denais et al., 2016; Jimenez et al.,

2014; Raab et al., 2016; Radulovic et al., 2018; Scheffer et al., 2014; Skowyra et al., 2018), as in a range of other membrane remodeling, budding, and fission phenomena (Christ et al., 2017; Hurley, 2015). These include formation of intraluminal vesicles of late endosomal multivesicular bodies (MVB) (Katzmann et al., 2002), budding of enveloped viruses including HIV (Dussupt et al., 2009; Fisher et al., 2007; Fujii et al., 2009; Garrus et al., 2001; Martin-Serrano et al., 2001), exosome formation (Baietti et al., 2012; Nabhan et al., 2012; van Niel et al., 2011), shedding of microvesicles or ectosomes (Choudhuri et al., 2014; Matusek et al., 2014; Nabhan et al., 2012), nuclear envelope reformation after mitosis (Olmos et al., 2015; Vietri et al., 2015), and for midbody abscission during cytokinesis (Carlton and Martin-Serrano, 2007; Morita et al., 2007). ESCRT play a role in repair of plasma membrane damaged by chemical or physical means (Jimenez et al., 2014; Scheffer et al., 2014), repair or removal of cell-death inducing plasma membrane pores in pyroptosis (Ruhl et al., 2018) or membrane disruption during necroptosis (Gong et al., 2017) repair of damaged lysosomes (Radulovic et al., 2018; Skowyra et al., 2018), repair of damaged nuclear envelope (Denais et al., 2016; Raab et al., 2016), and quality control and clearance of defective nuclear pores (Webster et al., 2014). One specific ESCRT component, ALIX, is capable of bypassing ESCRT-0/-I/-II during the recruitment of ESCRT-III proteins to membrane scission sites (Christ et al., 2017; Hurley, 2015). TSG101, an ESCRT-I component, and ALIX are recruited directly to membrane damage sites at lysosomes (Radulovic et al., 2018; Skowyra et al., 2018), nuclear envelope (Denais et al., 2016; Olmos et al., 2015; Raab et al., 2016; Vietri et al., 2015), and plasma membrane (Jimenez et al., 2014), and functional studies indicate that they may act redundantly during lysosomal damage repair (Radulovic et al., 2018; Skowyra et al., 2018). Among the latest additions to the portfolio of ESCRT roles (Christ et al., 2017; Hurley, 2015) is the final step of autophagosomal membrane closure, based on theoretical considerations and some experimental support suggesting that ESCRT-assisted membrane scission occurs between the future outer and inner membrane of closing phagophores to become fully sealed autophagosomes (Knorr et al., 2015; Lee et al., 2007; Rusten and Stenmark, 2009; Takahashi et al., 2018).

Autophagy is a process contributing to both cytoplasmic quality control and metabolism (Levine and Kroemer, 2019; Mizushima et al., 2011). This pathway can be activated by metabolic inputs or stress (Garcia and Shaw, 2017; Marino et al., 2014; Noda and Ohsumi, 1998; Saxton and Sabatini, 2017; Scott et al., 2004) or can also be selectively triggered by cargo recognition (Kimura et al., 2016; Lazarou et al., 2015; Mandell et al., 2014) when guided by autophagic receptors (Birgisdottir et al., 2013; Bjorkoy et al., 2005; Kimura et al., 2016; Levine and Kroemer, 2019; Stolz et al., 2014). Autophagy machinery is often recruited to damaged organelles after they are marked for degradation by ubiquitin or galectin tags (Randow and Youle, 2014; Stolz et al., 2014). Two well studied galectin-interacting autophagy receptors are NDP52 which recognizes galectin-8 (Gal8) (Thurston et al., 2012), and TRIM16, which binds to both galectin-3 (Gal3) (Chauhan et al., 2016) and Gal8 (Kimura et al., 2017). Autophagy initiation is controlled by several modules (Mizushima et al., 2011): (i) The ULK1/2 kinase complex with FIP200, ATG13 and ATG101, acting as conduits for inhibition by active mTOR (Ganley et al., 2009; Hosokawa et al., 2009; Jung et al., 2009) and activation by AMPK (Kim et al., 2011) to induce

autophagy; (ii) ATG14L-endowed Class III PI3-Kinase Complex (Baskaran et al., 2014; Chang et al., 2019; Petiot et al., 2000) that includes VPS34 and Beclin 1 (He and Levine, 2010), which can also be modified by AMPK to specifically activate the ATG14L form of VPS34 (Kim et al., 2013); (iii) the ATG5-ATG12/ATG16L1 E3 ligase conjugation system (Mizushima et al., 1998a; Mizushima et al., 1998b) lipidating mammalian Atg8 (mAtg8s), including LC3B, best known as a marker for autophagosomal membranes (Kabeya et al., 2000); (iv) ATG9, and the ATG2-WIPI protein complexes, of still unknown function (Bakula et al., 2017; Velikkakath et al., 2012; Young et al., 2006). These modules become interconnected, via FIP200 that bridges the ULK1/2 complex with the mAtg8s conjugation system by binding ATG16L1 (Fujita et al., 2013; Gammoh et al., 2013; Nishimura et al., 2013), via ATG16L1 and WIPI interactions (Dooley et al., 2014), and ATG13 connecting the ULK1/2 complex with ATG14-VPS34 (Jao et al., 2013; Park et al., 2016). After initiation, autophagy terminates in a merger of autophagosomes with degradative endolysosomal compartments whereby the sequestered cargo is degraded.

Galectins, which can act as tags for autophagy receptors (Chauhan et al., 2016; Thurston et al., 2012), are a family of cytosolically synthesized lectins with affinity for β-galactoside glycoconjugates, ubiquitously present in organisms from fungi to humans (Vasta et al., 2017), and in most cases sharing distinguishing characteristics as a group (Johannes et al., 2018; Nabi et al., 2015): (i) a common structure based on carbohydrate recognition domain (CRD) as the fundamental building block conserved in metazoans (Houzelstein et al., 2004), with molecular architecture variations in the number of tandem CRDs and one notable exception of Gal3 that has a long unique N-terminal domain attached to a single CRD (Johannes et al., 2018; Nabi et al., 2015). (ii) Galectins recognize galactose-containing glycans such as N-acetyllactosamine (Galβ1-3GlcNAc or Galβ1-4GlcNAc) on glycoconjugates (glycoproteins and potentially glycolipids) integral to exofacial or lumenal membranes of several intracellular organelles including lysosomes and plasma membrane as well as present in the extracellular matrix (Johannes et al., 2018). Galectins' glycan affinities start at the disaccharide level further influenced by sugar linkages and modifications, overall carbohydrate length, and glycoconjugate moiety context within N-linked glycosylated proteins and possibly O-linked glycoproteins and sphingolipids (Di Lella et al., 2011; Johannes et al., 2018). (iii) Galectins are unconventionally secreted (Stewart et al., 2017) and physiologically and medically have been mostly recognized and studied for their extracellular functions, with effects in cell adhesion, migration, signaling, inflammation, fibrosis, infection, diabetes, cancer, liver and heart disease (Di Lella et al., 2011; Johannes et al., 2018). Nevertheless, galectins have been reported to have some intracellular activities, including effects on Ras and Wnt signaling, interactions with Bcl-2 and a role in viral budding (Wang et al., 2014) and possibly exosome formation, as well as interactions with importins and pre-spliceosome complexes (Johannes et al., 2018). Galectins have been connected to autophagy initially as factors binding to autophagy receptors (Chauhan et al., 2016; Thurston et al., 2012). More recent studies have shown that galectins act in mTOR and AMPK signaling (Jia et al., 2018). Most of the intracellular activities of galectins have hitherto been considered neither interconnected nor integrated and are usually given as a list of disparate phenomena (Johannes et al., 2018).

Intracellular galectins are some of the best markers of endolysosomal damage since they form discernible puncta on damaged lysosomes (Aits et al., 2015). However, their specific functions on lysosomes are not fully understood and galectins are considered as tags or eat me signals involved in recognition of membrane damage. Here we show that Gal3 goes beyond being a marker of lysosomal damage (Aits et al., 2015) and that it recruits, controls and integrates several subsystems including ESCRT and autophagy pathways resulting in a coordinated set of steps within the multi-tiered cellular response to endomembrane damage. This response includes membrane repair, removal and replacement and, as identified here and elsewhere, is controlled by galectins.

RESULTS

Galectin-3 and ESCRT component ALIX interact and protect lysosomes from damage

Gal3 has been reported to function during lysosomal damage involving autophagy but kinetics of its response has not been determined and only one effector, TRIM16 has been identified so far (Chauhan et al., 2016). When we quantified Gal3 cytoplasmic puncta formation using high content microscopy (HCM), Gal3 response was already detectable at 30 min of treatment with lysosomal membrane damaging agent Leu-Leu-OMe (LLOMe) (Aits et al., 2015; Thiele and Lipsky, 1990) (Fig. 1A), and its response persisted for several hours afterwards (Figs. 1A and S1A). In a search for candidate effectors interacting with Gal3, we employed proteomic analyses using proximity biotinylation employing the engineered ascorbate peroxidase probe APEX2 (Lam et al., 2015) fused with Gal3 combined with liquid chromatography tandem mass spectrometry (LC/MS/MS) and DIA (EncyclopeDIA/scaffoldDIA) (Fig. 1B) (Searle et al., 2018). Among the interactors identified by LC/MS/MS (Fig. 1B. Table S1, Tabs 1 and 2), we found in three independent experiments comparing untreated controls with LLOMe-treated cells, several ESCRT proteins, including components of ESCR-0, ESCRT-I, and ESCRT-III and Bro1 domain family members (Christ et al., 2017; Hurley, 2015). Among those, the ESCRT protein PDCD6IP also known as ALIX (Hurley and Hanson, 2010) stood out as showing biggest fold-increase in becoming associated with Gal3 (Fig. 1B). ALIX, a component of the ESCRT machinery (Henne et al., 2011), forms puncta on lysosomes immediately following damage (Radulovic et al., 2018; Skowyra et al., 2018). ALIX, synergistically with the ESCRT-I component TSG101, recruits ESCRT-III components leading to membrane repair early during lysosomal damage (Radulovic et al., 2018; Skowyra et al., 2018). Based on the proteomic findings, we tested whether Gal3 and ALIX interact and how their interaction is affected during lysosomal damage. The levels of endogenous ALIX co-IP-ed with Gal3 increased at 30 min and peaked at 1 h after LLOMe treatment (Figs. 1C and S1B). In contrast to increased ALIX-Gal3 interactions at 30 min time point during LLOMe treatment, we observed diminishing interactions between GFP-Gal3 and endogenous TSG101 or FLAG-TSG101 as the lysosomal damage progressed (Figs. 1C, S1C and S1D). Nevertheless, early at 10 min, Gal3-TSG101 interactions persisted, before appreciable recruitment of ALIX (Fig. S1C). The overlaps between TSG101 and Gal3, biochemically detected here, could not be visualized in resting cells since Gal3 did not make any discernible profiles/puncta in untreated cells. These experiments were carried out with the standard human NCBI version of Gal3 (NP_002297.2), which contains only a partial P(S/

T)AP TSG101 binding motif (Gal3^{PSAT}). We found by BLAST searches human natural polymorphic variants with a complete P(S/T)AP motif (Gal3^{PSAP}), commonly found in monkeys and other species (Table S1, Tab 3). With Gal3^{PSAP} we detected an appreciable amount of GFP-TSG101 in co-IPs, but this interaction was also diminished, as with Gal3^{PSAT}, upon LLOMe treatment (Fig. S1E). Thus, of the ESCRT components ALIX and TSG101 implicated in the repair of lysosomal damage (Radulovic et al., 2018; Skowyra et al., 2018), ALIX selectively associates with Gal3 during lysosomal damage, although some overlaps between TSG101 and Gal3 have been reported by microscopy at early time points (Radulovic et al., 2018) compatible with biochemical observations of interactions between TSG101 and Gal3 detected herein.

By super-resolution microscopy (direct stochastic optical reconstruction microscopy), cellular regions were observed where GFP-Gal3 and ALIX colocalized (Figs. 1D and S1F), albeit some of the profiles contained only one marker (Fig. 1D, asterisk). Gal3-ALIX association was quantified by HCM and overlaps between Gal3 and ALIX increased during LLOMe treatment (Fig. S1G) with kinetics similar to that of the biochemical analyses above. We furthermore isolated lysosomal organelles by LysoIP methodology via HA-tagged TMEM192 (Abu-Remaileh et al., 2017) (Fig. 1E). The affinity purified lysosomal membranes contained ALIX and Gal3 only after LLOMe-inflicted damage. Thus, Gal3 and ALIX interact, colocalize, and co-recruit to damaged lysosomal organelles.

We tested whether Gal3 and ALIX play a role early in protection against lysosomal damage, using established assays for lysosomal quality and repair including LysoTracker Red (LTR) for lysosomal acidification, and Magic Red (MR), an in situ fluorescent reporter for measuring active cathepsin-B (Jia et al., 2018; Radulovic et al., 2018; Skowyra et al., 2018). In Gal3^{KO} HeLa cells (Jia et al., 2018) (Fig. 1F) or HeLa cells knocked down for ALIX (ALIX^{KD}) (Fig. 1G), there was a reduction in LTR^{+} profiles (quantified by HCM) at 30 min of LLOMe (Figs. 1F, 1G, S1H and S1I). During washout of LLOMe, LTR^{+} profiles recovered, but less efficiently in Gal3^{KO} and ALIX^{KD} cells (Figs. 1F, 1G, S1H and S1I). The MR^{+} profiles were reduced (HCM quantification) in Gal3^{KO} and ALIX^{KD} HeLa cells relative to wild type (WT) HeLa cells or HeLa cells treated with control/scrambled siRNA, respectively (Figs. S1J and S1K). Recovery of MR^{+} profiles were evident after LLOMe washout and it diminished in Gal3^{KO} and ALIX^{KD} HeLa cells (Figs. S1J and S1K), as with the LTR^{+} marker. Thus, ALIX, an ESCRT factor implicated in lysosomal damage repair (Radulovic et al., 2018; Skowyra et al., 2018), and Gal3 colocalize on damaged lysosomes and are both required for early protection against lysosomal damage (Fig. 1H).

To further determine the protection role of Gal3 at intermediate times during lysosomal damage, we overexpressed Gal3 (HeLa Flp-In-Gal3^{TetON}, Fig. S2A). When Gal3 expression was induced by tetracycline, Gal3 conferred super-protection against acute LLOMe damage or during LLOMe washout (Fig. S2A). By comparison with Gal3, knockouts of two other galectins, Gal8 and galectin-9 (Gal9), shown to play a role in mTOR inactivation and AMPK activation leading up to autophagy (Jia et al., 2018) did not affect lysosomal status during damage for 30 min, or recovery from damage (Figs. S2C and S2D), and Gal8 overexpression did not confer super-protection (Fig. S2B). To establish that Gal3 protected lysosomal damage, we used additional chemical (glycyl-L-phenylalanine 2-naphthylamide, GPN)

(Berg et al., 1994) and physical/mechanical (silica) (Hornung et al., 2008) agents. We observed similar requirement for Gal3 in protection against GPN (Fig. S2E) and silica (Fig. S2F). Thus, Gal3 plays a role in protection against lysosomal damage as revealed by assays and approaches applied to measure lysosomal membrane repair (Radulovic et al., 2018; Skowyra et al., 2018) at early and, as shown here, at intermediate time points (Fig. S2G).

Galectin-3 is required for efficient recruitment of ALIX to damaged lysosomes

We asked the question whether Gal3 is important for ALIX recruitment to damaged lysosomes. We used biochemical assay, i.e. LysoIP methodology, to determine whether Gal3 was required for ALIX recruitment. ALIX was strongly increased on LysoIP-purified lysosomes from Gal3 WT HeLa cells but not from Gal3^{KO} HeLa cells and only a minor ALIX increase was detected in the absence of Gal3 (Fig. 2A). In contrast to dependence of ALIX on Gal3 (Fig. 2A), TSG101, which was also detected on LysoIP-purified damaged lysosomes (Fig. 1E), its presence on damaged lysosomes was independent of Gal3 (Fig. 2A). Next, ALIX overlap with LAMP1 was quantified by HCM. Whereas the initial increase of ALIX detectable as early as 10 min was not affected in Gal3^{KO} HeLa cells, at 30 min the further increase in ALIX recruitment to LAMP1 organelles was abrogated in Gal3^{KO} HeLa cells (Figs. 2B and S2H). In contrast, the ramping up of ALIX levels on damaged lysosomes continued in Gal8^{KO} (Fig. S2H). Thus, Gal3, but not Gal8 previously shown to play a different albeit important role in affecting mTOR and autophagy (Jia et al., 2018), is required for efficient recruitment of ALIX to damaged lysosomes. We confirmed these observations using other lysosomal damaging agents, silica and tau oligomers, with latter reported recently to cause lysosomal damage (Papadopoulos et al., 2017). ALIX recruitment to lysosomes was diminished in Gal3^{KO} HeLa cells relative to WT cells in response to either of the agents (Figs. 2C and 2D). Thus, Gal3 is required for efficient ALIX recruitment to damaged lysosomes (Fig. 2E).

Glycosylation is important for galectin-3 recognition of lysosomal damage

Does Gal3 role in ALIX recruitment to lysosomes depend on recognition of damage-exposed lysosomal glycoconjugates? First, we compared effects of lysosomal damage in Lec3.2.8.1 mutant CHO cells with WT CHO cells. Lec3.2.8.1 lack complete N-glycans, which are major ligands for Gal3 (Patnaik et al., 2006), due to defects in Golgi transporters including UDP-Gal transporter and inability to trim the 5-mannose core to 3-mannose core en route to eventual additions of galactose residues (North et al., 2010; Patnaik and Stanley, 2006). Lec3.2.8.1 cells were more sensitive to LLOMe at 30 min of treatment and had diminished recovery from lysosomal damage upon washout (Fig. 3A). Gal3 and ALIX responses to LLOMe were diminished in Lec3.2.8.1 CHO cells relative to WT CHO cells (Figs. S3A and S3B). Thus, glycosylation is important for recruitment of ALIX and Gal3 to damaged lysosomes.

We next complemented Gal3^{KO} HeLa cells with WT Gal3 and Gal3^{R186S} mutant, previously shown to lose the ability to form cytoplasmic puncta in response to lysosomal damage (Aits et al., 2015), ascertained here by HCM quantification (a threefold drop in puncta formation in response to LLOMe; Fig. S3C). ALIX recruitment to LAMP1^{+} profiles was restored in Gal3^{KO} cells complemented with WT Gal3, but not with the Gal3^{R186S} (Fig. 3B). Likewise,

lysosomal function was protected (LTR HCM assay) by WT Gal3 but not with Gal3^{R186S} in complementation experiments (Fig. S3D). These observations are in keeping with glycosylation-dependent and Gal3-dependent damage recognition/signaling being important for ALIX recruitment to damaged lysosomes, where it can perform a repair function as previously shown (Radulovic et al., 2018; Skowyra et al., 2018).

Proteomic analysis of proteins recognized by galectin-3 during lysosomal damage

To determine which lysosomal glycoproteins are recognized by Gal3 to signal lysosomal damage and engage effectors described above, we carried out a dynamic proteomic analysis by proximity biotinylation. We identified and compared Gal3 interactors by LC/MS/MS using APEX2-Gal3 fusion under control and lysosomal damage (GPN and LLOMe) conditions, for a total of three independent experiments (Table S1, Tab 4). Surprisingly, among glycosylated proteins within the endolysosomal system we did not find anticipated candidates as potential Gal3 interactors, e.g. PSAP, GNS and TMEM192 glycoproteins previously reported to be exposed and ubiquitinated during lysosomal damage (Yoshida et al., 2017) or SLC38A9 that we found as a specific interactor of Gal8 during lysosomal damage (Jia et al., 2018). However, one unanticipated candidate stood out, transferrin receptor protein 1 (TFRC). TFRC showed a >10-fold increase following lysosomal damage by spectral counts in LC/MS/MS (Fig. S3E and Table S1, Tab4), which were carried out in addition to the DIA LC/MS/MS data in Fig. 1B and Table S1, Tab2. Both the DIA (peak intensities) and DDA (spectral counts) data from dynamic proximity biotinylation with APEX2-Gal3 indicated significant increase in Gal3-TFRC interactions upon lysosomal damage (Fig. S3F). We next employed LysoIP to test whether TFRC becomes detectable within lysosomes following damage. TFRC was increased in affinity purified lysosomes after 30 min of LLOMe treatment (Fig. 3C). This was unexpected, since TFRC is usually associated with early and recycling endosomes (Dautry-Varsat et al., 1983; Maxfield and McGraw, 2004). TFRC could traverse endosomal system to lysosomes under other stress conditions, as it was found in increased amounts in affinity purified lysosomes in starved cells as well (Fig. 3C), suggesting that under stress conditions TFRC penetrates deeper into the endolysosomal continuum and reaches lysosomes. This is in keeping with a report that inhibition of mTOR by starvation and rapamycin can cause TFRC redistribution to lysosomes (Dauner et al., 2017). By HCM quantification, TFRC and LAMP2 overlap increased upon damage (Fig. S3G), and so did the overlap between TFRC and Gal3 (Fig. S3H). Gal3-TFRC formed protein complexes, detected by co-IP, and these interactions increased during lysosomal damage (Fig. 3D). The increased interaction between Gal3 and TFRC in cells treated with LLOMe depended on the ability of Gal3 to recognize damage-exposed glycan as evidenced by reduced levels of TFRC, which is a known glycosylated protein (Do et al., 1990; McClelland et al., 1984), in co-IPs with Gal3^{R186S} relative to co-IPs with WT Gal3 (Fig. 3E).

We tested whether TFRC was functionally important for Gal3 recruitment to damaged lysosomes. For this, we knocked down TFRC, and measured the effects on Gal3 colocalization with LAMP1 in LLOMe-treated cells, which showed reduced overlap in TFRC^{KD} cells relative to control siRNA cells (Fig. 3F). Next, we tested whether TFRC was also required for efficient ALIX recruitment to lysosomes. ALIX recruitment to damaged

lysosomes was reduced in TFRC^{KD} cells (Fig. 3G). There was nevertheless a residual Gal3 and ALIX recruitment to lysosomes in TFRC^{KD} cells which can be ascribed to contributions by additional glycans, e.g. those on LAMP2 (see volcano plot in Table S1, Tab2). TFRC^{KD} cells also showed increased sensitivity to LLOMe-induced damage assessed by stronger loss of LysoTracker staining (Fig. S3I).

ALIX colocalization with TFRC depended on Gal3 (Fig. 3H), whereas Gal3 did not affect TFRC relocation to lysosomes during damage (Fig. S4A). In complementation experiments expressing GFP-Gal3 and its mutant GFP-Gal3^{R186S}, only the wild type Gal3 that recognizes exposed glycans restored colocalization between ALIX and TFRC elicited by lysosomal damage (Fig. S4B). Knockdown of TFRC in Gal3^{KO} cells did not further reduce ALIX recruitment to lysosomes by LysoIP (Fig. 3I) and HCM analyses (Fig. S4C) during LLOMe treatment, confirming that they act on the same pathway for ALIX recruitment to damaged lysosomes. Other lysosomal proteins, such as LAMP2, showed increased interactions with Gal3 by dynamic proteomic analyses, similarly to TFRC in LLOMe treated cells (Table S1, Tab2). Nevertheless, when we knocked down TFRC it completely abrogated ALIX association with Gal3 by co-IPs, suggesting a key role for TFRC in Gal3-ALIX binding (Fig. S4D). Thus, TFRC, a glycosylated protein and a Gal3 interacting partner, which associates with Gal3 upon lysosomal damage, is important for Gal3 and ALIX recruitment during cellular response to lysosomal injury (Fig. S4E).

Optimal ALIX recruitment to damaged lysosomes requires two signals

Previous work implicated Ca^{2+} signaling in the recruitment of ALIX to damaged lysosomes (Skowyra et al., 2018). We tested the contribution of Ca^{2+} vs additional mechanisms using BAPTA-AM for intracellular chelation of Ca^{2+} as previously applied (Skowyra et al., 2018). We observed that at 10 min, most of ALIX recruitment was abrogated. At 30 min of LLOMe treatment, ALIX recruitment increased despite Ca^{2+} chelation albeit some Ca^{2+}-dependence persisted (Fig. 4A). We then checked Gal3 response, and it increased in the presence of BAPTA-AM (Fig. 4B). When we tested Gal3-ALIX interaction by co-IP, we observed a very strong increase in ALIX-Gal3 complexes in the presence of Ca^{2+} chelator (Fig. 4C). ALIX recruitment to lysosomes was quantified by HCM and whereas Ca^{2+} was important so was Gal3 in the absence or presence of Ca^{2+} (Fig. 4D) indicating that Gal3 is important as a Ca^{2+}- independent recruiter of ALIX to damaged lysosomes. The effects of calcium and Gal3 could be temporally separated, because when we compared effects of BAPTA-AM at 10 min of LLOMe treatment in WT and Gal3^{KO} HeLa cells, ALIX recruitment to LAMP1 organelles was equally reduced in both cases (Fig. 4E), indicating that at 10 min upon damage, ALIX's recruitment depends primarily on Ca^{2+} and not on Gal3. This was confirmed by LysoIP, which showed that only BAPTA-AM suppressed ALIX recruitment to lysosomes at 10 min of LLOMe exposure and that Gal3^{KO} did not affect this phase of ALIX response (Fig. 4F) whereas at 30 min both BAPTA-AM and Gal3^{KO} affected levels of ALIX recruitment (Fig. 4G). These relationships quantified by HCM and confirmed biochemically by LysoIP, are summarized in Fig. 4H and are illustrated in live microscopy observations (Movies. S1-4).

Galectin-3 promotes sequential aspects of ESCRT response to lysosomal damage

We tested recruitment of ESCRT-III machinery downstream of ALIX to damaged lysosomes, using LysoIP methodology. By LysoIP lysosomal purification we detected CHMP4A and CHMP4B accumulation on damaged lysosomes at 30 min of LLOMe treatment (Figs. 5A(i)-(iii)). This was not the case in $Gal3^{KO}$ cells at 30 min (Figs. 5A(i)-(iii)). Some levels of CHMP4A and CHM4B were detectable on lysosomes at 10 min of damage and were independent of Gal3 (Figs. 5B(i)-(iii)). Imaging quantification by HCM of the overlap between CHMP4A and endogenous LAMP1 indicated that at 10 min of LLOMe treatment only BAPTA-AM affected CHMP4A recruitment and that $Gal3^{KO}$ had no effects (Fig. S5A). However, at 30 min of LLOMe treatment, $Gal3^{KO}$ reduced CHMP4A recruitment to lysosomes (Fig. S5B). This is further illustrated in live microscopy observations (Movie S5). CHMP4A and CHMP4B were found by co-IP in complexes with Gal3 at increasing amounts during 10-30 min of LLOMe treatment and remained at high levels at 1 h (Figs. 5C(i)-(ii) and 5D). Upon LLOMe treatment, ALIX and CHMP4B showed increased association by co-IP and this was further augmented by co-expression of GFP-Gal3 (Fig 5E). Conversely, ALIX-CHMP4B association was reduced in $Gal3^{KO}$ cells (Fig. 5F). When we complemented $Gal3^{KO}$ cells with WT Gal3 or its mutant $Gal3^{R186S}$, only WT Gal3 rescued ALIX-CHMP4B association (Fig. 5G), showing that the effect of Gal3 on formation of ALIX-CHMP4B complexes is dependent on the ability of Gal3 to recognize damaged lysosomes (Fig. S3C). Thus, Gal3 facilitated formation of complexes between ALIX and CHMP4B specifically on damaged lysosomes. We found that CHMP4A and CHMP4B were in complexes with Gal3, and this depended on a complete Gal3 as deletion of either the N-terminal domain of Gal3 or C-terminal CRD of Gal3 diminished association (Figs. S5C-E). Thus, not only does Gal3 recruit ALIX to sites of lysosomal damage but it facilitates transition to ESCRT-III complex formation (Fig. S5F).

Galectin-3 is important for autophagy response in systems causing lysosomal damage

We previously reported that galectins act not only as tags for selective autophagy (Thurston et al., 2012), but that they affect autophagy at multiple levels including organization of autophagy initiation complexes (Chauhan et al., 2016) and as direct regulators of the upstream kinases mTOR and AMPK, which control autophagy (Jia et al., 2018). Gal3 has been indirectly implicated in autophagy but a requirement for Gal3 in autophagy response to lysosomal injury has not been determined in Gal3 knockout cells (Chauhan et al., 2016). We tested the subsequently reported $Gal3^{KO}$ cells (Jia et al., 2018) and examined formation of ATG13 puncta, the earliest precursors of autophagosomes in mammalian cells related to the ULK1 complex formation (Ganley et al., 2009; Hosokawa et al., 2009; Jung et al., 2009; Karanasios et al., 2013; Karanasios et al., 2016; Meijer et al., 2007). We found by HCM a reduced number of ATG13 puncta per cell in $Gal3^{KO}$ cells relative to WT cells in response to lysosomal damage (Fig. 6A). This was also reflected in diminished ATG16L1 and LC3 puncta in $Gal3^{KO}$ cells relative to WT cells (Figs. 6B and 6C). In complementation experiments, WT Gal3 restored ATG13, ATG16L1 and LC3 puncta formation response, whereas the glycan recognition mutant $Gal3^{R186S}$ did not (Fig. 6D-F). Thus, Gal3 is important in a glycan recognition-dependent fashion for autophagy induction in response to lysosomal damage.

Galectin-3 contributes to a switch between ESCRT response and autophagy during endomembrane damage

We have previously shown that Gal3 interacts with TRIM16 (Chauhan et al., 2016), a cargo receptor-organizer of autophagy initiation machinery during lysosomal damage. We thus asked a question whether Gal3 sequentially participates in ESCRT-driven repair and TRIM16-driven autophagy events. Given that Gal3 acts earlier during lysosomal damage in combination with ESCRT (i.e., ALIX peaked at 1h and diminished at 2 h of LLOMe treatment; Fig. S1B), we wondered about the timing of Gal3 engagement with TRIM16. We found that TRIM16 in FLAG-Gal3 complexes only increased at 2 h of LLOMe treatment, whereas ALIX and another ESCRT protein CHMP4B decreased in the same complexes (Fig. 7A). A similar trend was observed for TRIM16 and Gal3 complex in stable HeLa Flp-In-Gal3^{TetON} cells (Fig. S5G). The Gal3 CRD domain but not the N-terminal domain of Gal3 formed specific complexes with TRIM16 (Figs. S5E and S5H), reverse of the domain requirement for Gal3 interactions with ALIX, which depends on the N-terminal domain of Gal3 (Wang et al., 2014). Further, when we knocked down ALIX in HeLa Flp-In-Gal3^{TetON}, we observed increased association of TRIM16 with Gal3, whereas overexpression of ALIX decreased TRIM16-Gal3 complexes (Figs. 7B and 7C). ALIX and Gal3 showed increased association in TRIM16^{KO} cells and conversely, ALIX-Gal3 association was reduced by co-expression of GFP-TRIM16 (Figs. 7D and 7E). Thus, Gal3 switches from ESCRT interactions, implicated in membrane repair (Radulovic et al., 2018; Skowyra et al., 2018), to TRIM16 interactions, implicated in autophagic removal of damaged lysosomes (Chauhan et al., 2016) (Fig. S5I).

Autophagy has been implicated in control of intracellular *Mycobacterium tuberculosis* (*Mtb*) (Gutierrez et al., 2004). The details of this control are yet to be fully determined, but the host-pathogen interactions are known to be driven by the ability of *Mtb* to cause endomembrane damage (Castillo et al., 2012; Manzanillo et al., 2012; Watson et al., 2012). A connection between Gal3 and *Mtb* protection has been established, although its effectors have not been investigated (Chauhan et al., 2016). Previously, using Gal3^{KO} mice, we have shown increased susceptibility in models of *Mtb* infection both ex vivo in bone marrow-derived macrophages (BMMs) and in vivo in *Mtb* aerosol-infected Gal3^{KO} mice (Chauhan et al., 2016). Here, we generated a transgenic conditional KO mouse (see STAR methods) for the Gal3 effector TRIM16 involved in autophagy. The resulting TRIM16$^{fl/fl}$ mouse was crossed with the LysM-Cre driver to delete TRIM16 in myeloid lineage. We then tested *Mtb* control in BMMs from TRIM16$^{fl/fl}$ LysM-Cre^{-} vs LysM-Cre^{+} littermates. When autophagy was induced in *Mtb*-infected macrophages, BMMs from TRIM16$^{fl/fl}$ LysM-Cre^{+} mice showed reduced control of *Mtb* relative to TRIM16$^{fl/fl}$LysM-Cre^{-} littermates (Fig. S5J). Furthermore, when mice were tested in the aerosol infection model of acute *Mtb* infection (Chauhan et al., 2016; Jia et al., 2018), the TRIM16$^{fl/fl}$ LysM-Cre^{+} showed higher susceptibility in early stages postinfection (Fig. S5K). Thus, both Gal3 (Chauhan et al., 2016) and its autophagy effector TRIM16 manifest their roles in biological outputs of autophagy in systems known to cause endomembrane damage.

We next tested connections between different components of the response associated with lysosomal damage, including ALIX-dominated repair and autophagy. When membrane

repair was rendered inefficient by knocking down ALIX, autophagy was increased as measured by ATG13 and ATG16L1 puncta formation (Figs. S6A and S6B). Conversely, when lysophagy was inefficient, as in TRIM16^{KO} (Chauhan et al., 2016), this heightened ALIX response to lysosomal damage (Fig. S6C). Both ALIX and TRIM16/autophagy are effectors of Gal3, as shown here for ALIX and previously reported for TRIM16 (Chauhan et al., 2016). In keeping with this Gal3^{KO} inhibited both ALIX (Fig. 2) and autophagy (Fig. 6) responses, albeit this was temporally resolved, indicating a switch. The roles of other galectins reported to respond to lysosomal damage, Gal8 and Gal9, are also integrated in this process as Gal8 and Gal9 inhibit mTOR and activate AMPK, respectively, following lysosomal damage (Fig. S6F) (Jia et al., 2018). Gal8 and Gal9 (puncta formation) was increased in Gal3^{KO} cells (Figs. S6D and S6E), indicating that reduction in ESCRT-based lysosomal damage repair increased Gal8 and Gal9 responses. TFEB, a transcription factor controlling lysosomal biogenesis via its translocation form the cytoplasm to the nucleus (Medina et al., 2015; Napolitano and Ballabio, 2016), has been shown to respond to lysosomal damage (Chauhan et al., 2016; Jia et al., 2018). TFEB nuclear translocation, which increases as recently shown (Chauhan et al., 2016) during lysosomal damage, was increased in Gal3^{KO} cells at each time point tested (Fig. 7F). Thus, galectins coordinate various stages of response to lysosomal damage and bridge ESCRT repair phase with autophagy and TFEB response (Figs. 7G and S6F).

DISCUSSION

In this study, we have defined a set of coordinated activities, orchestrated in part by Gal3, which are deployed by cells to counter lysosomal damage through ESCRT-dependent repair, autophagy-dependent removal, and eventual replacement through activation of lysosomal biogenesis. Whereas the individual elements of this response, such as ESCRT-based membrane repair (Radulovic et al., 2018; Skowyra et al., 2018), autophagy of damaged lysosomes (Fujita et al., 2013; Maejima et al., 2013; Yoshida et al., 2017), and TFEB activation (Chauhan et al., 2016; Jia et al., 2018) have been appreciated, our study now connects these activities into a harmonized homeostatic system of integrated pathways. The role of coordinating different parts of this system belongs to galectins, which are recognized here as regulators of cellular response for membrane repair, removal and replacement. This concept aligns with our earlier studies (Chauhan et al., 2016; Jia et al., 2018) and studies by others (Aits et al., 2015; Feeley et al., 2017; Thurston et al., 2012; Wang et al., 2014) and assigns a very specific function to intracellular galectins as active regulators of endomembrane homeostasis. This is linked to the general ability of galectins to recognize membrane damage through binding to glycans exposed on exofacial (lumenal) leaflets of organellar membranes and their ability to sequentially recruit and activate or inactivate downstream effectors.

Gal3, the principal focus of the present study, recruits ALIX at intermediate time points following early calcium-dominated recruitment of ALIX to damaged lysosomes. The calcium-dependent recruitment of ALIX may be based on Ca^{2+}-sensitive ALIX interactors such ALG-2 reported as being recruited early to damaged lysosomes (Skowyra et al., 2018). However, ALG-2 functional role remains to be established (Skowyra et al., 2018) and thus any studies of the effects of ALG-2 and lysosomal calcium stores on Gal3 action in this

context would have to be addressed in separate studies. At later times, Gal3 switches to the recruitment of autophagy machinery. This is consistent with the previously reported drop in ALIX on damaged lysosomes, while Gal3 persists even at much later time points (Skowyra et al., 2018) when Gal3 switches its interactions from ALIX to TRIM16 as shown here.

Galectins have different binding partners that dynamically change during lysosomal damage. ALIX, as shown in this work and previously (Wang et al., 2014) and TRIM16 (Chauhan et al., 2016) sequentially associate with Gal3, through interactions that are direct. In the case of Gal8, it interacts with SLC38A9 plus parts of the Ragulator complex (Jia et al., 2018), whereas Gal9 activates AMPK (Jia et al., 2018), all acting during response to lysosomal damage. Surprisingly, different galectins have almost exquisite specificity for different glycosylated proteins on lysosomes that they recognize as homing signals for recognition of lysosomal membrane changes. For example, Gal8 binds exclusively (MASSIVE accession MSV000081788) to SLC38A9 after lysosomal damage but not to other lysosomal proteins (Jia et al., 2018) implicated in recognition by glycan-homing E3 ligases such as FBXO27 (Yoshida et al., 2017). Gal3, based on our proteomic analyses here, is not in a vicinity of SLC38A9, but instead associates with TFRC. Gal3-TFRC association increased during lysosomal damage, and although TFRC is typically in early and recycling endosomal compartments, we found by LysoIP and HCM that it penetrates deeper into the endolysosomal continuum and thus can act as a reporter of lysosomal damage to Gal3. In addition, this indicates that Gal3 could patrol for damage in other parts of the endo-lysosomal pathway. The glycan-recognizing ubiquitin ligase FBXO27 interacts with TFRC (Glenn et al., 2008; Yoshida et al., 2017) and then ubiquitinates a number of lysosomal proteins (LAMP1, LAMP2, PSAP, GNS, TMEM192), en route to lysophagy (Yoshida et al., 2017). TFRC engagement has also been seen on endosomes (or rather phagosomes and macropinosomes) damaged by small latex beads coated with a transfection agent (Yoshida et al., 2017). Thus, TFRC seems to be a frequently utilized signal for detection by the exposed glycan-recognizing systems.

We show a key role of Gal3 in recruitment of ALIX, an ESCRT component that bridges ESCRT-I and ESCRT-III and connects upstream partners and regulators with the downstream ESCRT-III machinery (Christ et al., 2017; Hurley, 2015). Although ALIX and TSG101 have been considered as redundant in membrane damage repair (Hurley, 2015; Jimenez et al., 2014; Radulovic et al., 2018; Ruhl et al., 2018; Skowyra et al., 2018), they act as two separate branches of the ESCRT pathway that lead to the common ESCRT-III and VPS4 effectors involved in membrane scission (Hurley, 2015). Here we found that ALIX and TSG101 show temporal separation in their interactions with Gal3 following membrane damage. Consistent with this, downregulation of ALIX alone in our experiments increased sensitivity to damage as detected by lysosomal function. Since TSG101 showed reduced interaction with Gal3 and our focus was on Gal3-ALIX associations, we did not investigate relative contributions of TSG101 vs ALIX. We nevertheless note that data shown by Skowyra et al. (Skowyra et al., 2018) indicate that ALIX is important for the overall ESCRT action measured by the recruitment of CHMP4A.

Gal3 sequences/orders different parts of the sequential responses with specific molecular switches as evidenced in the observed interdependence of Gal3-ALIX vs. Gal3-TRIM16

interactions and Gal3 enabling interactions between different components of the ESCRT machinery such as ALIX-CHMP4B association, which is a key step for ESCRT function in membrane repair as shown previously. These and other aspects of Gal3 action, are also dependent on its recognizing exposed glycans, and represent a relatively understudied signal transduction process. The roles of galectins in endomembrane homeostasis and autophagy are multifaceted, as depicted in models in Figs. 7G and S6F. One of the first functions recognized was Gal8 serving as a passive tag to detect Salmonella-damaged vesicles and recruit an autophagy receptor NDP52 (Thurston et al., 2012). Later on, Gal8 has been assigned an additional, more active role, by controlling mTOR and being responsible for its inactivation during lysosomal damage (Jia et al., 2018). This occurs in the course of lysosomal damage via increased binding of Gal8 to SLC38A9 and Ragulator components thus affecting Rag GTPases and inhibiting mTOR activity (Jia et al., 2018). Gal9 also responds to lysosomal damage, but its interactors on lysosomal membrane are not known at present. Nevertheless, it activates AMPK during lysosomal injury (Jia et al., 2018). Together, inactivation of mTOR and activation of AMPK promote autophagy induction. Whereas Gal3 early on works with ESCRT, it later on assumes a second function through its direct interactor TRIM16 by scafolding components of autophagy initiation machinery including ULK1, Beclin 1 and ATG16L1 (Chauhan et al., 2016), thus driving autophagosomal membrane formation in response to damage. This explains why Gal3 is such a good marker of damaged lysosomes relative to other galectins, in alignment with its ubiquitous and strong expression (Aits et al., 2015). Here we also firmed up the role of Gal3-TRIM16 in significant biological outputs such as control of phagocytosed *Mtb.* Furthermore, we show in the mouse model of *Mtb* infection that TRIM16 matters for protection against aerosol infection with this pathogen similarly to the previously shown role of Gal3 in protection against *Mtb* in vivo (Chauhan et al., 2016). Others have recently reported in a *Dictyostelium discoideum-Mycobacterium marinum* model a role for ESCRT and autophagy in intracellular bacterial control (Lopez-Jimenez et al., 2018), with indications that the two aspects are coordinated, however with no mechanistic insights into how these responses may be connected. It is possible that analogous systems may regulate transitions in *D. discoideum* similar to the responses described herein. We did not specifically investigate whether Gal3 also participates at the autophagosome closure stage via its interacting partners such as ALIX, and it is possible that Gal3 or other factors contribute to these late events as well.

The final stage of the responses studied here is a lysosome replacement program through lysosomal biogenesis. This occurs through activation of TFEB, which increases expression of numerous lysosomal genes and is directly controlled by mTOR (Martina et al., 2012; Martina and Puertollano, 2013; Medina et al., 2015; Napolitano and Ballabio, 2016; Roczniak-Ferguson et al., 2012; Settembre et al., 2011; Settembre et al., 2012). The mTOR inhibition exerted via Gal8 and Gal9 (Jia et al., 2018) and the role of TRIM16 in mTOR inactivation and its effects on TFEB during autophagy phase (Chauhan et al., 2016) all contribute to the lysosomal replacement program.

It is likely that components of endomembrane homeostasis ensure a graded response to damage, and that repair, removal and replacement are coordinated to either cope and repair damage or escalate response due to accumulation of unsalvageable organelles. The

biological and medical significance of this cannot be overstated given the fact that lysosomes, endosomes, phagosomes, autophagosomes, autolysosomes and other membranous organelles play roles in a wide range of physiological and pathological states, including inflammation, infection, fibrosis, tissue and muscle atrophy, neurodegeneration, metabolic disorders and cancer.

STAR METHODS

Contact for Reagent and Resource Sharing

Further information and requests for resources and reagents should be directed to and will be fulfilled by the Lead Contact, Vojo Deretic (vderetic@salud.unm.edu). All unique/stable reagents generated in this study are available from the Lead Contact with a completed Materials Transfer Agreement negotiated as governed by the University of New Mexico and state requirements and, where applicable, covering costs associated with preparation and shipping.

Experimental Models and Subject Details

Mice—The generation of TRIM16fl/fl mouse founders directly in the C57BL/6 background was conducted by Cyagen. It involved mouse genomic fragment amplification from a BAC clone by using high fidelity Taq polymerase, and their sequential assembly into a targeting vector together with recombination sites and selection markers. The linearized vector was delivered to ES cells (C57BL/6) via electroporation, followed by drug selection, PCR screening and Southern blot detection. After confirming correctly targeted ES clones via Southern blotting, clones were selected for blastocyst microinjection, followed by chimera production. Founders were confirmed as germline-transmitted via crossbreeding with wild-type. TRIM16$^{fl/fl}$ mice were bread with LysM-Cre C57BL/6 mice. Littermates for experiments were generated by breading TRIM16$^{fl/fl}$ LysM-Cre^{+} mice with TRIM16$^{fl/fl}$ mice to generate Cre^{+} and Cre^{-} littermates thus accounting for metagenomic considerations. Mice were 4-10 weeks old and included both sexes equally and near-equally represented in experimental groups. Genotyping was through Transnetyx services. All breeding procedures have been carried out following protocols approved by IACUC.

Cell and cell line models—Murine bone marrow derived macrophages (BMMs; primary cells) and authenticated cell lines were used for *Murine tuberculosis* infection analyses. Cell types, lines and culture conditions are described under Method Details.

Murine tuberculosis* infection model—Mycobacterium tuberculosis* Erdman (Manzanillo et al., 2012) were cultured in Middlebrook 7H9 broth supplemented with 0.05% Tween 80, 0.2% glycerol, and 10% oleic acid, albumin, dextrose, and catalase (OADCBD Biosciences) at 37°C and homogenized to generate single-cell suspension for macrophage infection studies. Mice were exposed to *Mtb* Erdman aerosols (intermediate dose of 1,372 CFU initial lung deposition as previously defined (Chauhan et al., 2016)) using a GlasCol apparatus for aerosol delivery, and survival monitored for 100 days post infection. All procedures have been carried out under ABSL3 conditions, following protocols approved by

IACUC, and adherence to approved protocols was monitored by an independent direct observer.

Method Details

Antibodies and reagents—Antibodies from Abcam were Galectin-3 (ab53082) (1:1000 for Western blot (WB); 1:200 for immunofluorescence (IF)), GFP (ab290) (1:1000 for WB), GFP (ab38689) (2/mL for immunoprecipitation (IP)), mCherry (ab183628) (1:1000 for WB; 1:200 for IF; 2 μg/mL for IP), VDAC1(ab15895) (1:1000 for WB), CHMP4B(ab105767) (1:1000 for WB),CHMP4A (ab67058)(1:1000 for WB), GM130(ab1299) (1:1000 for WB), P4HB(ab2792)(1:1000 for WB) and TSG101(ab83) (1:1000 for WB). Antibodies from MBL International were LC3(PM036) (1:500 for IF) and ATG16L1(PM040) (1:400 for IF). Antibodies from BioLegend were Galectin-3 (#125402) (1:1000 for WB; 1:500 for IF) and ALIX (#634502) (1:1000 for WB; 1:400 for IF). Antibodies from Cell Signaling Technology were TFEB (#4240) (1:200 for IF), ATG13 (#13468) (1:200 for IF) and LAMP1(#9091) (1:500 for IF). Other antibodies used in this study were from the following sources: FLAG M2 (F1804) (1:1000 for WB) from Sigma Aldrich; TRIM16(A301-160A) (1:1000 for WB) from Bethyl; Myc (sc-40) (1:200 for WB), Galectin-8 (sc-28254) (1:200 for WB) and beta-Actin (C4) (1:1000 for WB), HRP-labeled anti-rabbit(1:2000 for WB) and anti-mouse (1:2000 for WB) secondary antibodies from Santa Cruz Biotechnology; LAMP2 (H4B4) (1:500 for IF) from DSHB of University of Iowa; Clean-Blot IP Detection Kit (HRP) (21232) (1:1000 for WB), Alexa Fluor 488, 568 (1:500 for IF), TFRC(#13-6800) (1:1000 for WB, 1:200 for IF) from ThermoFisher Scientific. DMEM, RPMI and EBSS medias from Life Technologies.

Cells and cell lines—HEK293T, HeLa and huh7 cells were from ATCC. Bone marrow derived macrophages (BMMs) were isolated from femurs of TRIM16$^{fl/fl}$ LysM-Cre mice and its Cre-negative litermates cultured in DMEM supplemented with mouse macrophage colony stimulating factor (mM-CSF, #5228, CST). HeLa Flp-In-Gal3^{TetON} were generated using constructs from Terje Johansen. Cell lines for LysoIP were generated using constructs obtained from David M. Sabatini (Whitehead Institute). CHO and Lec3.2.8.1 cells were from Pamela Stanley (Albert Einstein College of Medicine).

Plasmids, siRNAs, and transfection—Plasmids used in this study, such as ALIX and CHMP4A cloned into pDONR221 using BP cloning, and expression vectors were made utilizing LR cloning (Gateway, ThermoFisher) in appropriate pDEST vectors for immunoprecipitation assay.

Gal3 mutants were generated utilizing the QuikChange site-directed mutagenesis kit (Agilent) and confirmed by sequencing (Genewiz). siRNAs were from GE Dharmacon. Plasmid transfections were performed using the ProFection Mammalian Transfection System (Promega) or Amaxa nucleofection (Lonza). siRNAs were delivered into cells using either Lipofectamine RNAiMAX (ThermoFisher Scientific) or Amaxa nucleofection (Lonza).

Generation of HeLa Flp-In-Gal3^{TetON} cell line—Transfect Hela Flp-In host cells with Gal3 reconstructed plasmid and the pOG44 expression plasmid at ration of 9:1. 24 h after transfection, wash the cells and add fresh medium to the cells. 48 h after transfection, split the cells into fresh medium around 25 % confluent. Incubate the cells at 37 °C for 2–3 h until they have attached to the culture dish. Then them medium was removed and added with fresh medium containing 100 μg/mL hygromycin. Feed the cells with selective medium every 3–4 days until single cell clone can be identified. Pick hygromycin-resistant clones and expand each clone to test. The tested clones incubated in the medium containing 1 μg/mL tetracycline overnight were determined by western blot for the expressing of Gal3.

Generation of LysM-Cre TRIM16$^{fl/fl}$ mice—The generation of TRIM16fl/fl mouse founders directly in the C57BL/6 background was conducted by Cyagen. It involved mouse genomic fragment amplification from a BAC clone by using high fidelity Taq polymerase, and their sequential assembly into a targeting vector together with recombination sites and selection markers. The linearized vector was delivered to ES cells (C57BL/6) via electroporation, followed by drug selection, PCR screening and Southern blot detection. After confirming correctly targeted ES clones via Southern blotting, clones were selected for blastocyst microinjection, followed by chimera production. Founders were confirmed as germline-transmitted via crossbreeding with wild-type. TRIM16$^{fl/fl}$ mice were bread with LysM-Cre C57BL/6 mice. Littermates for experiments were generated by breading TRIM16$^{fl/fl}$ LysM-Cre^{+} mice with TRIM16$^{fl/fl}$ mice to generate Cre^{+} and Cre^{-} littermates thus accounting for metagenomic considerations.

LysoTracker assay—Prepare fresh LysoTracker Staining Solution (2 μL LysoTracker in 1mL medium). Add 10 μL LysoTracker Staining Solution to no treatment, 1 mM LLOMe treated or LLOMe washout cells in 96 wells for total 100 μL per well and incubate at 37 °C for 30 min protected from light. Rinse gently by 1X PBS and fix in 4 % Paraformaldehyde for 2min. Wash once by 1X PBS and blot with Hoechst 33342 for 2 min before detecting by high content microscopy.

Magic Red assay—Reconstitute Magic Red by adding DMSO and dilute Magic Red 1:10 by adding H_2O. Add 4 μL Magic Red to no treatment, 1 mM LLOMe treated or LLOMe washout cells in 96 wells for total 100 μL per well and incubate at 37 °C for 15 min and protected from light. Rinse gently by 1X PBS and fix in 4 % Paraformaldehyde for 2 min. Wash once by 1X PBS and blot with Hoechst 33342 for 2 min before detecting by high content microscopy.

LysoIP assay—HEK293T cells were transfected with pLJC5-TMEM192-3xHA or pLJC5-TMEM192-2XFLAG constructs in combination with pCMV-VSV-G and psPAX2 packaging plasmids, 60 h after transfection, the supernatant containing lentiviruses was collected and centrifuged to remove cells and then frozen at −80°C. To establish LysoIP stably expressing cell lines, HEK293T, HeLa or HeLa Gal3^{KO} cells were plated in 10cm dish in DMEM with 10 % FBS and infected with 500μL of virus-containing media overnight, then add puromycin for selection.

Cells in 15 cm plates with 90 % confluency were used for each LysoIP. Cells with or without 1 mM LLOMe treatment were quickly rinsed twice with PBS and then scraped in1mL of KPBS (136 mM KCl, 10 mM KH_2PO_4, pH7.25 was adjusted with KOH) and centrifuged at 3000 rpm for 2 min at 4 °C. Pelleted cells were resuspended in 950 μL KPBS and reserved 25 μL for further processing of the whole-cell lysate. The remaining cells were gently homogenized with 20 strokes of a 2 mL homogenizer. The homogenate was then centrifuged at 3000 rpm for 2 min at 4 °C and the supernatant was incubated with 100 μL of KPBS prewashed anti-HA magnetic beads (ThermoFisher) on a gentle rotator shaker for 3 min. Immunoprecipitants were then gently washed three times with KPBS and eluted with 2×Laemmli sample buffer (Bio-Rad) and subjected to immunoblot analysis.

High content microscopy—Cells in 96 well plates were treated, followed by fixation in 4 % paraformaldehyde for 5 min. Cells were then permeabilized with 0.1 % saponin in 3 % Bovine serum albumin (BSA) for 30 min followed by incubation with primary antibodies for 2 h and secondary antibodies for 1h. High content microscopy with automated image acquisition and quantification was carried out using a Cellomics HCS scanner and iDEV software (ThermoFisher Scientific). Automated epifluorescence image collection was performed for a minimum of 500 cells per well. Epifluorescence images were machine analyzed using preset scanning parameters and object mask definitions. Hoechst 33342 staining was used for autofocus and to automatically define cellular outlines based on background staining of the cytoplasm. Primary objects were cells, and regions of interest (ROI) or targets were algorithm-defined by shape/segmentation, maximum/minimum average intensity, total area and total intensity, etc., to automatically identify puncta or other profiles within valid primary objects. Nuclei were defined as a region of interest for TFEB translocation. All data collection, processing (object, ROI, and target mask assignments) and analyses were computer driven independently of human operators.

Super-resolution imaging and analysis—Super-resolution imaging and analysis were done as described previously(Kumar et al., 2018; Pallikkuth et al., 2018). HeLa cells transfected with GFP-Gal3 were plated on 25 mm round #1.5 coverslips (Warner Instruments) coated with Poly-L-Lysine solution (Sigma-Aldrich) and allowed to adhere overnight. After two steps fixation (first step (0.6 % PFA, 0.1 % Glyoxal solution (GA), 0.2 5% Triton X-100) for 60 sec; second step (4 % PFA, 0.2 % GA) for 3 h), cells were washed by 1xPBS twice, and incubated with 0.1 % NaBH4 for 5 min. After washed by 1xPBS twice, cells were incubated with 10 mM Tris for 5 min, then block cells with 5 %BSA containing 0.05 % Triton X-100 for 15 min. After washed by 1xPBS once, cells were incubated with anti–rabbit-GFP antibody for 2 h and washed with 1xPBS three times followed by labeling with Alexa Fluor 647 (A21245, Invitrogen). The coverslip was mounted on an Attofluor cell chamber (A-7816, ThermoFisher Scientific) with 1.1 mL of the imaging buffer. Imaging buffer consisted of an enzymatic oxygen-scavenging system and primary thiol: 50 mM Tris, 10 mM NaCl, 10 % (wt/vol) glucose, 168.8 U/mL glucose oxidase (G2133, Sigma-Aldrich), 1,404 U/mL catalase (C9332, Sigma-Aldrich), and 20 mM 2-aminoethanethiol, pH8. The chamber was sealed by placing an additional coverslip over the chamber, and the oxygen-scavenging reaction was allowed to proceed for 20 min at room temperature before the imaging started.

Imaging was performed using a custom-built microscope controlled by custom-written software (github.com/LidkeLab/matlab-instrument-control) in MATLAB (MathWorks Inc.). The samples were loaded on an *xyz* piezo stage (Mad City Labs, Nano-LPS100) mounted on a manual *x-y* translator. Images were recorded on an iXon 897 electron-multiplying charge coupled (EMCCD) camera (Andor Technologies, South Windsor, CT). The EMCCD gain was set to 100, and 256x256 pixel frames were collected with a pixel resolution of 0.1078 mm. A 642-nm laser (collimated from a laser diode, HL6366DG, Thorlabs) was used for sample excitation. The laser was coupled into a multi-mode fiber (P1-488PM-FC-2, Thorlabs) and focused onto the back focal plane of the objective lens (UAPON 150XOTIRF, Olympus America Inc.). Sample excitation was done through a quad-band dichroic and filter set (LF405/488/561/635-A; Semrock, Rochester, NY). Fluorescence emission path included a band-pass filter (685/45, Brightline) and a quadband optical filter (Photometrics, QV2-SQ) with 4 filter sets (600/37,525/45,685/40,445/45, Brightline).

When imaging the first label (GFP-Gal3), for each target cell a brightfield reference image was saved in addition to the *x-y* stage position coordinates. The 642-nm laser was used at ~1 kW/cm2 to take 20 sets of 2,000 frames (a total of 40,000) at 60 Hz. After imaging all target cells, imaging buffer was replaced with 1xPBS, the residual fluorescence was photobleached, quenched with NaBH4 and washed thrice with 1xPBS. Before the second round of imaging, cells were blocked for 30 min, labeled with anti-ALIX antibody (#634502, BioLegend) for 1 h, washed with 1XPBS three times and relabeled using an Alexa Fluor 647 conjugated anti-mouse antibody at 10 μg/mL for 1 h. Before the second round of imaging, each target cell was located and realigned using the saved brightfield reference image as described in (Valley et al., 2015).

Data were analyzed via a 2D localization algorithm based on maximum likelihood estimation (Smith et al., 2010). The localized emitters were filtered through thresholds of maximum background photon counts of 200, minimum photon counts per frame per emitter of 250, and a data model hypothesis test (Huang et al., 2011) with a minimum p-value of 0.01. The accepted emitters were used to reconstruct the super-resolution image. Each emitter was represented by a 2D Gaussian function with σ_x and σ_y equal to the localization precisions, which were calculated from the Cramér-Rao Lower Bound (CRLB). Clustering analysis was performed with MATLAB code using clustering tools (http://stmc.health.unm.edu/tools-and-data/). Several regions of interest (ROIs) were selected from the image. Clustering was then performed separately for each label in each ROI using the density-based DBSCAN algorithm choosing a maximal nearest neighbor distance of 40 nm and requiring clusters to contain at least 5 observations. In all cases, most observations for each label in each ROI formed a single cluster. Cluster boundaries were produced via the MATLAB “boundary” function, from which inter-label cluster distances were computed.

Time-lapse imaging of cultured cells—Wild type or Gal3^{KO} HeLa cell expressing mCherry-ALIX and GFP-LAMP1, were treated with 15μM BAPTA-AM for 1h and then incubated with 1mM LLOMe for live-cell fluorescence image which was performed using an inverted microscope (confocal TCS SP5,Leica, LAS AF version 2.6.0), a 63x PlanAPO oil-immersion objective lens (NA 1.4). Two-color time-lapse images were acquired at 340 ms intervals and z-stacks collapsed into 2D projections to generate movies.

Co-immunoprecipitation assay—Cells transfected with 8-10 μg of plasmids were lysed in NP-40 buffer (ThermoFisher Scientific) supplemented with protease inhibitor cocktail (Roche, 11697498001) and 1 mM PMSF (Sigma, 93482) for 30 min on ice. Supernatants were incubated with (2-3 μg) antibodies overnight at 4°C. The immune complexes were captured with Dynabeads (ThermoFisher Scientific), followed by three times washing with 1X PBS. Proteins bound to Dynabeads were eluted with 2×Laemmli sample buffer (Bio-Rad) and subjected to immunoblot analysis.

APEX2-labeling and streptavidin enrichment for immunoblotting analyses—HEK293T cells transfected pJJiaDEST-APEX2-Gal3 were incubated with 100 μM GPN (Cayman Chemicals) or 1 mM LLOMe in full medium for 1 h (confluence of cells remained at 70-80 %). Cells were next incubated in 500 μM biotin-phenol (AdipoGen) in full medium for the last 45 min of GPN or LLOMe incubation. A 1 min pulse with 1 mM H_2O_2 at room temperature was stopped with quenching buffer (10 mM sodium ascorbate, 10 mM sodium azide and 5 mM Trolox in Dulbecco's Phosphate Buffered Saline (DPBS)). All samples were washed twice with quenching buffer, and twice with DPBS.

For LC/MS/MS analysis, cell pellets were lysed in 500 μL ice-cold lysis buffer (6 M urea, 0.3 M Nacl, 1 mM EDTA, 1 mM EGTA, 10 mM sodium ascorbate, 10 mM sodium azide, 5 mM Trolox, 1 % glycerol and 25 mm Tris/HCl, PH 7.5) for 30 min by gentle pipetting. Lysates were clarified by centrifugation and protein concentrations determined as above. Streptavidin–coated magnetic beads (Pierce) were washed with lysis buffer. 3 mg of each sample was mixed with 100 μL of streptavidin bead. The suspensions were gently rotated at 4 °C for overnig ht to bind biotinylated proteins. The flowthrough after enrichment was removed and the beads were washed in sequence with 1 mL IP buffer (150 mM NaCl, 10 mM Tris-HCl pH8.0, 1 mM EDTA, 1 mM EGTA, 1 % Triton X-100) twice; 1 mL 1M KCl; 1mL of 50 mM Na_2CO_3; 1 mL 2M Urea in 20 mM Tris HCl pH8; 1 mL IP buffer. Biotinylated proteins were eluted, 10 % of the sample processed for Western Blot and 90 % of the sample processed for mass spectrometry.

Protein samples on magnetic beads were washed four times with 200ul of 50mM Triethyl ammonium bicarbonate (TEAB) with a 20 minutes shake time at 4 °C in between each wash. Roughly 2.5 μg of trypsin was added to the bead and TEAB mixture and the samples were digested over night at 800 rpm shake speed. After overnight digestion the supernatant was removed, and the beads were washed once with enough 50 mM ammonium bicarbonate to cover. After 20 minutes at a gentle shake the wash is removed and combined with the initial supernatant. The peptide extracts are reduced in volume by vacuum centrifugation and a small portion of the extract is used for fluorometric peptide quantification (Thermo scientific Pierce). One microgram of sample based on the fluorometric peptide assay was loaded for each LC/MS analysis.

LC/MS/MS DDA—Digested peptides were analyzed by LC/MS/MS on a Thermo Scientific Q Exactive Plus Orbitrap Mass spectrometer in conjunction Proxeon Easy-nLC II HPLC (Thermo Scientific) and Proxeon nanospray source. The digested peptides were loaded a 100-micron x 25 mm Magic C18 100A 5U reverse phase trap where they were desalted online before being separated using a 75-micron x 150 mm Magic C18 200Å 3U reverse

phase column. Peptides were eluted using a 140 min gradient with a flow rate of 300 nL/min. An MS survey scan was obtained for the m/z range 350-1600, MS/MS spectra were acquired using a top 15 method, where the top 15 ions in the MS spectra were subjected to HCD (High Energy Collisional Dissociation). An isolation mass window of 1.6 m/z was for the precursor ion selection, and normalized collision energy of 27 % was used for fragmentation. A fifteen-second duration was used for the dynamic exclusion.

LC/MS/MS DIA—Peptides were separated on an Easy-spray 100 μm x 25 cm C18 column using a Dionex Ultimate 3000 nUPLC. Solvent A=0.1 % formic acid, Solvent B=100 % Acetonitrile 0.1 % formic acid. Gradient conditions = 2 %B to 50 %B over 60 minutes, followed by a 50 %-99 % B in 6 minutes and then held for 3 minutes than 99 %B to 2 %B in 2 minutes. Total Run time = 90 minutes. Thermo Scientific Fusion Lumos mass spectrometer running in Data independent Analysis mode. Two gas phases fractionated (GFP) injections were made per sample using sequential 4 Da isolation widows. GFP1 = m/z 362-758, GFP 2 = m/z 758-1158. Tandem mass spectra were acquired using a collision energy of 30, resolution of 30K, maximum inject time of 54 ms and a AGC target of 50K.

DDA quantification and statistical analysis—Mass spectrometry data processing and analysis were done as described previously (Jia et al., 2018). Tandem mass spectra were extracted by Proteome Discoverer version 2.2. Charge state deconvolution and deisotoping were not performed. All MS/MS samples were analyzed using Sequest-HT (XCorr Only) (Thermo Fisher Scientific, San Jose, CA, USA; in Proteome Discoverer 2.2.0.388). Sequest (XCorr Only) was set up to search the gpm common laboratory contaminants and the Uniprot human proteome 3AUP000005640 with isoforms (Aug 2017, 93299 entries) assuming the digestion enzyme trypsin. Sequest (XCorr Only) was searched with a fragment ion mass tolerance of 0.020 Da and a parent ion tolerance of 10.0 PPM. Carbamidomethyl of cysteine was specified in Sequest (XCorr Only) as a fixed modification. Deamidated of asparagine, oxidation of methionine and acetyl of the n-terminus were specified in Sequest (XCorr Only) as variable modifications. Precursor intensity was determined using Proteome Discoverer 2.2 using the Minora Feature detector with the default options.

Scaffold (version Scaffold_4.8.2, Proteome Software Inc., Portland, OR) was used to validate MS/MS based peptide and protein identifications. Peptide identifications were accepted if they could be established at greater than 93.0 % probability to achieve an FDR less than 0.1 % by the Scaffold Local FDR algorithm. Protein identifications were accepted if they could be established at greater than 99.0 % probability and contained at least two identified peptides. This filtering resulted in a decoy false discovery rate of 0.08 % on the spectra level and 0.7 % on the protein level. Protein probabilities were assigned by the Protein Prophet algorithm. Proteins that contained similar peptides and could not be differentiated based on MS/MS analysis alone were grouped to satisfy the principles of parsimony. Proteins sharing significant peptide evidence were grouped into clusters. Raw data and ScaffoldDIA results are available from the MassIVE proteomics repository (MSV000083998) and Proteome Exchange PXD014304. Reviewer password for Proteome Exchange = Galectin3.

DIA quantification and statistical analysis—DIA data was analyzed using Scaffold DIA (1.3.1). Raw data files were converted to mzML format using ProteoWizard (3.0.11748). Analytic samples were aligned based on retention times and individually searched against *Pan human library* http://www.swathatlas.org/ with a peptide mass tolerance of 10.0 ppm and a fragment mass tolerance of 10.0 ppm. Variable modifications considered were: Modification on M M and Modification on C C. The digestion enzyme was assumed to be Trypsin with a maximum of 1 missed cleavage site(s) allowed. Only peptides with charges in the range <2..3> and length in the range <6..30> were considered. Peptides identified in each sample were filtered by Percolator (3.01.nightly-13-655e4c7-dirty) to achieve a maximum FDR of 0.01. Individual search results were combined and peptide identifications were assigned posterior error probabilities and filtered to an FDR threshold of 0.01 by Percolator (3.01. nightly-13-655e4c7-dirty).

Peptide quantification was performed by Encyclopedia (0.8.1). For each peptide, the 5 highest quality fragment ions were selected for quantitation. Proteins that contained similar peptides and could not be differentiated based on MS/MS analysis were grouped to satisfy the principles of parsimony. Proteins with a minimum of 2 identified peptides were thresholded to achieve a protein FDR threshold of 1.0%. Raw data and ScaffoldDIA results are available from the MassIVE proteomics repository (MSV000083998) and Proteome Exchange PXD014304. Reviewer password for Proteome Exchange = Galectin3.

Data and code availability

Original microscopy and Western blots of this study have been deposited at Mendeley data http://dx.doi.org/10.17632/v52k86mp58.1: Raw MS DIA/DDA data have been deposited at the MassIVE proteomics repository (MSV000083998) and Proteome Exchange PXD014304.

Quantification and Statistical Analysis

Data in this study are presented as means ± SEM ($n \geq 3$). Data were analyzed with either analysis of variance (ANOVA) with Tukey's HSD post-hoc test, or a two-tailed Student's *t* test. For HCM, $n \geq 3$ includes in each independent experiment: 500 valid primary objects/cells per well, from ≥ 5 wells per plate per sample. Animal survival data were analyzed by log-rank (Mantel-Cox) method. Statistical significance was defined as: † (not significant) $p \geq 0.05$ and *$p < 0.05$, **$p < 0.01$.

Supplementary Material

Refer to Web version on PubMed Central for supplementary material.

ACKNOWLEDGMENTS

We thank D. Sabatini for LysoIP constructs, K. Bhaskar for tau oligomers, and M. Wester for mathematical analysis of super resolution results. Mass spectrometry analysis, BP and MS were supported by NIH Shared instrumentation grant 1S10OD021801. KL was supported by NIH grants 1R21EB019589, P50GM085273, P30CA118100. This work was supported by NIH grants R37AI042999 and R01AI042999 and center grant P20GM121176 to V.D.

REFERENCES

Abu-Remaileh M, Wyant GA, Kim C, Laqtom NN, Abbasi M, Chan SH, Freinkman E, and Sabatini DM (2017). Lysosomal metabolomics reveals V-ATPase- and mTOR-dependent regulation of amino acid efflux from lysosomes. Science 358, 807–813. [PubMed: 29074583]

Aits S, Kricker J, Liu B, Ellegaard AM, Hamalisto S, Tvingsholm S, Corcelle-Termeau E, Hogh S, Farkas T, Holm Jonassen A, et al. (2015). Sensitive detection of lysosomal membrane permeabilization by lysosomal galectin puncta assay. Autophagy 11, 1408–1424. [PubMed: 26114578]

Baietti MF, Zhang Z, Mortier E, Melchior A, Degeest G, Geeraerts A, Ivarsson Y, Depoortere F, Coomans C, Vermeiren E, et al. (2012). Syndecan-syntenin-ALIX regulates the biogenesis of exosomes. Nat Cell Biol 14, 677–685. [PubMed: 22660413]

Bakula D, Muller AJ, Zuleger T, Takacs Z, Franz-Wachtel M, Thost AK, Brigger D, Tschan MP, Frickey T, Robenek H, et al. (2017). WIPI3 and WIPI4 beta-propellers are scaffolds for LKB1-AMPK-TSC signalling circuits in the control of autophagy. Nature communications 8, 15637.

Baskaran S, Carlson LA, Stjepanovic G, Young LN, Kim do J, Grob P, Stanley RE, Nogales E, and Hurley JH (2014). Architecture and dynamics of the autophagic phosphatidylinositol 3-kinase complex. Elife 3.

Berg TO, Stromhaug E, Lovdal T, Seglen O, and Berg T (1994). Use of glycyl-L-phenylalanine 2-naphthylamide, a lysosome-disrupting cathepsin C substrate, to distinguish between lysosomes and prelysosomal endocytic vacuoles. Biochem J 300 (Pt 1), 229–236. [PubMed: 8198538]

Birgisdottir AB, Lamark T, and Johansen T (2013). The LIR motif - crucial for selective autophagy. Journal of cell science 126, 3237–3247. [PubMed: 23908376]

Bjorkoy G, Lamark T, Brech A, Outzen H, Perander M, Overvatn A, Stenmark H, and Johansen T (2005). p62/SQSTM1 forms protein aggregates degraded by autophagy and has a protective effect on huntingtin-induced cell death. J Cell Biol 171, 603–614. [PubMed: 16286508]

Carlton JG, and Martin-Serrano J (2007). Parallels between cytokinesis and retroviral budding: a role for the ESCRT machinery. Science 316, 1908–1912. [PubMed: 17556548]

Castillo EF, Dekonenko A, Arko-Mensah J, Mandell MA, Dupont N, Jiang S, Delgado-Vargas M, Timmins GS, Bhattacharya D, Yang H, et al. (2012). Autophagy protects against active tuberculosis by suppressing bacterial burden and inflammation. Proceedings of the National Academy of Sciences of the United States of America 109, E3168–3176. [PubMed: 23093667]

Chang C, Young LN, Morris KL, von Bulow S, Schoneberg J, Yamamoto-Imoto H, Oe Y, Yamamoto K, Nakamura S, Stjepanovic G, et al. (2019). Bidirectional Control of Autophagy by BECN1 BARA Domain Dynamics. Mol Cell 73, 339–353 e336. [PubMed: 30581147]

Chauhan S, Kumar S, Jain A, Ponpuak M, Mudd MH, Kimura T, Choi SW, Peters R, Mandell M, Bruun JA, et al. (2016). TRIMs and Galectins Globally Cooperate and TRIM16 and Galectin-3 Co-direct Autophagy in Endomembrane Damage Homeostasis. Dev Cell 39, 13–27. [PubMed: 27693506]

Choudhuri K, Llodra J, Roth EW, Tsai J, Gordo S, Wucherpfennig KW, Kam LC, Stokes DL, and Dustin ML (2014). Polarized release of T-cell-receptor-enriched microvesicles at the immunological synapse. Nature 507, 118–123. [PubMed: 24487619]

Christ L, Raiborg C, Wenzel EM, Campsteijn C, and Stenmark H (2017). Cellular Functions and Molecular Mechanisms of the ESCRT Membrane-Scission Machinery. Trends Biochem Sci 42, 42–56. [PubMed: 27669649]

Dauner K, Eid W, Raghupathy R, Presley JF, and Zha X (2017). mTOR complex 1 activity is required to maintain the canonical endocytic recycling pathway against lysosomal delivery. The Journal of biological chemistry 292, 5737–5747. [PubMed: 28196862]

Dautry-Varsat A, Ciechanover A, and Lodish HF (1983). pH and the recycling of transferrin during receptor-mediated endocytosis. Proc Natl Acad Sci U S A 80, 2258–2262. [PubMed: 6300903]

Denais CM, Gilbert RM, Isermann P, McGregor AL, te Lindert M, Weigelin B, Davidson PM, Friedl P, Wolf K, and Lammerding J (2016). Nuclear envelope rupture and repair during cancer cell migration. Science 352, 353–358. [PubMed: 27013428]

Di Lella S, Sundblad V, Cerliani JP, Guardia CM, Estrin DA, Vasta GR, and Rabinovich GA (2011). When galectins recognize glycans: from biochemistry to physiology and back again. Biochemistry 50, 7842–7857. [PubMed: 21848324]

Do SI, Enns C, and Cummings RD (1990). Human transferrin receptor contains O-linked oligosaccharides. The Journal of biological chemistry 265, 114–125. [PubMed: 2403553]

Dooley HC, Razi M, Polson HE, Girardin SE, Wilson MI, and Tooze SA (2014). WIPI2 Links LC3 Conjugation with PI3P, Autophagosome Formation, and Pathogen Clearance by Recruiting Atg12-5-16L1. Mol Cell 55, 238–252. [PubMed: 24954904]

Dupont N, Lacas-Gervais S, Bertout J, Paz I, Freche B, Van Nhieu GT, van der Goot FG, Sansonetti PJ, and Lafont F (2009). Shigella phagocytic vacuolar membrane remnants participate in the cellular response to pathogen invasion and are regulated by autophagy. Cell Host Microbe 6, 137–149. [PubMed: 19683680]

Dussupt V, Javid MP, Abou-Jaoude G, Jadwin JA, de La Cruz J, Nagashima K, and Bouamr F (2009). The nucleocapsid region of HIV-1 Gag cooperates with the PTAP and LYPXnL late domains to recruit the cellular machinery necessary for viral budding. PLoS Pathog 5, e1000339. [PubMed: 19282983]

Feeley EM, Pilla-Moffett DM, Zwack EE, Piro AS, Finethy R, Kolb JP, Martinez J, Brodsky IE, and Coers J (2017). Galectin-3 directs antimicrobial guanylate binding proteins to vacuoles furnished with bacterial secretion systems. Proc Natl Acad Sci U S A 114, E1698–E1706. [PubMed: 28193861]

Fisher RD, Chung HY, Zhai Q, Robinson H, Sundquist WI, and Hill CP (2007). Structural and biochemical studies of ALIX/AIP1 and its role in retrovirus budding. Cell 128, 841–852. [PubMed: 17350572]

Fujii K, Munshi UM, Ablan SD, Demirov DG, Soheilian F, Nagashima K, Stephen AG, Fisher RJ, and Freed EO (2009). Functional role of Alix in HIV-1 replication. Virology 391, 284–292. [PubMed: 19596386]

Fujita N, Morita E, Itoh T, Tanaka A, Nakaoka M, Osada Y, Umemoto T, Saitoh T, Nakatogawa H, Kobayashi S, et al. (2013). Recruitment of the autophagic machinery to endosomes during infection is mediated by ubiquitin. J Cell Biol 203, 115–128. [PubMed: 24100292]

Gammoh N, Florey O, Overholtzer M, and Jiang X (2013). Interaction between FIP200 and ATG16L1 distinguishes ULK1 complex-dependent and -independent autophagy. Nat Struct Mol Biol 20, 144–149. [PubMed: 23262492]

Ganley IG, Lam du H, Wang J, Ding X, Chen S, and Jiang X (2009). ULK1.ATG13.FIP200 complex mediates mTOR signaling and is essential for autophagy. The Journal of biological chemistry 284, 12297–12305. [PubMed: 19258318]

Garcia D, and Shaw RJ (2017). AMPK: Mechanisms of Cellular Energy Sensing and Restoration of Metabolic Balance. Mol Cell 66, 789–800. [PubMed: 28622524]

Garrus JE, von Schwedler UK, Pornillos OW, Morham SG, Zavitz KH, Wang HE, Wettstein DA, Stray KM, Cote M, Rich RL, et al. (2001). Tsg101 and the vacuolar protein sorting pathway are essential for HIV-1 budding. Cell 107, 55–65. [PubMed: 11595185]

Glenn KA, Nelson RF, Wen HM, Mallinger AJ, and Paulson HL (2008). Diversity in tissue expression, substrate binding, and SCF complex formation for a lectin family of ubiquitin ligases. The Journal of biological chemistry 283, 12717–12729. [PubMed: 18203720]

Gong YN, Guy C, Olauson H, Becker JU, Yang M, Fitzgerald P, Linkermann A, and Green DR (2017). ESCRT-III Acts Downstream of MLKL to Regulate Necroptotic Cell Death and Its Consequences. Cell 169, 286–300 e216. [PubMed: 28388412]

Gutierrez MG, Master SS, Singh SB, Taylor GA, Colombo MI, and Deretic V (2004). Autophagy is a defense mechanism inhibiting BCG and Mycobacterium tuberculosis survival in infected macrophages. Cell 119, 753–766. [PubMed: 15607973]

He C, and Levine B (2010). The Beclin 1 interactome. Current opinion in cell biology 22, 140–149. [PubMed: 20097051]

Henne WM, Buchkovich NJ, and Emr SD (2011). The ESCRT pathway. Dev Cell 21, 77–91. [PubMed: 21763610]

Hornung V, Bauernfeind F, Halle A, Samstad EO, Kono H, Rock KL, Fitzgerald KA, and Latz E (2008). Silica crystals and aluminum salts activate the NALP3 inflammasome through phagosomal destabilization. Nat Immunol 9, 847–856. [PubMed: 18604214]

Hosokawa N, Hara T, Kaizuka T, Kishi C, Takamura A, Miura Y, Iemura S, Natsume T, Takehana K, Yamada N, et al. (2009). Nutrient-dependent mTORC1 association with the ULK1-Atg13-FIP200 complex required for autophagy. Mol Biol Cell 20, 1981–1991. [PubMed: 19211835]

Houzelstein D, Goncalves IR, Fadden AJ, Sidhu SS, Cooper DN, Drickamer K, Leffler H, and Poirier F (2004). Phylogenetic analysis of the vertebrate galectin family. Mol Biol Evol 21, 1177–1187. [PubMed: 14963092]

Huang F, Schwartz SL, Byars JM, and Lidke KA (2011). Simultaneous multiple-emitter fitting for single molecule super-resolution imaging. Biomed Opt Express 2, 1377–1393. [PubMed: 21559149]

Hurley JH (2015). ESCRTs are everywhere. EMBO J 34, 2398–2407. [PubMed: 26311197]

Hurley JH, and Hanson PI (2010). Membrane budding and scission by the ESCRT machinery: it's all in the neck. Nat Rev Mol Cell Biol 11, 556–566. [PubMed: 20588296]

Jao CC, Ragusa MJ, Stanley RE, and Hurley JH (2013). A HORMA domain in Atg13 mediates PI 3-kinase recruitment in autophagy. Proc Natl Acad Sci U S A 110, 5486–5491. [PubMed: 23509291]

Jia J, Abudu YP, Claude-Taupin A, Gu Y, Kumar S, Choi SW, Peters R, Mudd MH, Allers L, Salemi M, et al. (2018). Galectins Control mTOR in Response to Endomembrane Damage. Mol Cell 70, 120–135 e128. [PubMed: 29625033]

Jimenez AJ, Maiuri P, Lafaurie-Janvore J, Divoux S, Piel M, and Perez F (2014). ESCRT machinery is required for plasma membrane repair. Science 343, 1247136. [PubMed: 24482116]

Johannes L, Jacob R, and Leffler H (2018). Galectins at a glance. J Cell Sci 131.

Jung CH, Jun CB, Ro SH, Kim YM, Otto NM, Cao J, Kundu M, and Kim DH (2009). ULK-Atg13-FIP200 complexes mediate mTOR signaling to the autophagy machinery. Mol Biol Cell 20, 1992–2003. [PubMed: 19225151]

Kabeya Y, Mizushima N, Ueno T, Yamamoto A, Kirisako T, Noda T, Kominami E, Ohsumi Y, and Yoshimori T (2000). LC3, a mammalian homologue of yeast Apg8p, is localized in autophagosome membranes after processing. Embo J 19, 5720–5728. [PubMed: 11060023]

Karanasios E, Stapleton E, Manifava M, Kaizuka T, Mizushima N, Walker SA, and Ktistakis NT (2013). Dynamic association of the ULK1 complex with omegasomes during autophagy induction. J Cell Sci 126, 5224–5238. [PubMed: 24013547]

Karanasios E, Walker SA, Okkenhaug H, Manifava M, Hummel E, Zimmermann H, Ahmed Q, Domart MC, Collinson L, and Ktistakis NT (2016). Autophagy initiation by ULK complex assembly on ER tubulovesicular regions marked by ATG9 vesicles. Nature communications 7, 12420.

Katzmann DJ, Odorizzi G, and Emr SD (2002). Receptor downregulation and multivesicular-body sorting. Nat Rev Mol Cell Biol 3, 893–905. [PubMed: 12461556]

Kim J, Kim YC, Fang C, Russell RC, Kim JH, Fan W, Liu R, Zhong Q, and Guan KL (2013). Differential regulation of distinct Vps34 complexes by AMPK in nutrient stress and autophagy. Cell 152, 290–303. [PubMed: 23332761]

Kim J, Kundu M, Viollet B, and Guan KL (2011). AMPK and mTOR regulate autophagy through direct phosphorylation of Ulk1. Nat Cell Biol 13, 132–141. [PubMed: 21258367]

Kimura T, Jia J, Kumar S, Choi SW, Gu Y, Mudd M, Dupont N, Jiang S, Peters R, Farzam F, et al. (2017). Dedicated SNAREs and specialized TRIM cargo receptors mediate secretory autophagy. EMBO J 36, 42–60. [PubMed: 27932448]

Kimura T, Mandell M, and Deretic V (2016). Precision autophagy directed by receptor regulators - emerging examples within the TRIM family. J Cell Sci 129, 881–891. [PubMed: 26906420]

Knorr RL, Lipowsky R, and Dimova R (2015). Autophagosome closure requires membrane scission. Autophagy 11, 2134–2137. [PubMed: 26466816]

Kumar S, Jain A, Farzam F, Jia J, Gu Y, Choi SW, Mudd MH, Claude-Taupin A, Wester MJ, Lidke KA, et al. (2018). Mechanism of Stx17 recruitment to autophagosomes via IRGM and mammalian Atg8 proteins. J Cell Biol 217, 997–1013. [PubMed: 29420192]

Lam SS, Martell JD, Kamer KJ, Deerinck TJ, Ellisman MH, Mootha VK, and Ting AY (2015). Directed evolution of APEX2 for electron microscopy and proximity labeling. Nat Methods 12, 51–54. [PubMed: 25419960]

Lazarou M, Sliter DA, Kane LA, Sarraf SA, Wang C, Burman JL, Sideris DP, Fogel AI, and Youle RJ (2015). The ubiquitin kinase PINK1 recruits autophagy receptors to induce mitophagy. Nature 524, 309–314. [PubMed: 26266977]

Lee JA, Beigneux A, Ahmad ST, Young SG, and Gao FB (2007). ESCRT-III dysfunction causes autophagosome accumulation and neurodegeneration. Curr Biol 17, 1561–1567. [PubMed: 17683935]

Levine B, and Kroemer G (2019). Biological Functions of Autophagy Genes: A Disease Perspective. Cell 176, 11–42. [PubMed: 30633901]

Lopez-Jimenez AT, Cardenal-Munoz E, Leuba F, Gerstenmaier L, Barisch C, Hagedorn M, King JS, and Soldati T (2018). The ESCRT and autophagy machineries cooperate to repair ESX-1-dependent damage at the Mycobacterium-containing vacuole but have opposite impact on containing the infection. PLoS Pathog 14, e1007501. [PubMed: 30596802]

Maejima I, Takahashi A, Omori H, Kimura T, Takabatake Y, Saitoh T, Yamamoto A, Hamasaki M, Noda T, Isaka Y, et al. (2013). Autophagy sequesters damaged lysosomes to control lysosomal biogenesis and kidney injury. EMBO J 32, 2336–2347. [PubMed: 23921551]

Mandell MA, Jain A, Arko-Mensah J, Chauhan S, Kimura T, Dinkins C, Silvestri G, Munch J, Kirchhoff F, Simonsen A, et al. (2014). TRIM proteins regulate autophagy and can target autophagic substrates by direct recognition. Dev Cell 30, 394–409. [PubMed: 25127057]

Manzanillo PS, Shiloh MU, Portnoy DA, and Cox JS (2012). Mycobacterium Tuberculosis Activates the DNA-Dependent Cytosolic Surveillance Pathway within Macrophages. Cell host & microbe 11, 469–480. [PubMed: 22607800]

Marino G, Pietrocola F, Eisenberg T, Kong Y, Malik SA, Andryushkova A, Schroeder S, Pendl T, Harger A, Niso-Santano M, et al. (2014). Regulation of autophagy by cytosolic acetyl-coenzyme A. Mol Cell 53, 710–725. [PubMed: 24560926]

Martin-Serrano J, Zang T, and Bieniasz PD (2001). HIV-1 and Ebola virus encode small peptide motifs that recruit Tsg101 to sites of particle assembly to facilitate egress. Nat Med 7, 1313–1319. [PubMed: 11726971]

Martina JA, Chen Y, Gucek M, and Puertollano R (2012). MTORC1 functions as a transcriptional regulator of autophagy by preventing nuclear transport of TFEB. Autophagy 8, 903–914. [PubMed: 22576015]

Martina JA, and Puertollano R (2013). Rag GTPases mediate amino acid-dependent recruitment of TFEB and MITF to lysosomes. J Cell Biol 200, 475–491. [PubMed: 23401004]

Matusek T, Wendler F, Poles S, Pizette S, D'Angelo G, Furthauer M, and Therond PP (2014). The ESCRT machinery regulates the secretion and long-range activity of Hedgehog. Nature 516, 99–103. [PubMed: 25471885]

Maxfield FR, and McGraw TE (2004). Endocytic recycling. Nat Rev Mol Cell Biol 5, 121–132. [PubMed: 15040445]

McClelland A, Kuhn LC, and Ruddle FH (1984). The human transferrin receptor gene: genomic organization, and the complete primary structure of the receptor deduced from a cDNA sequence. Cell 39, 267–274. [PubMed: 6094009]

Medina DL, Di Paola S, Peluso I, Armani A, De Stefani D, Venditti R, Montefusco S, Scotto-Rosato A, Prezioso C, Forrester A, et al. (2015). Lysosomal calcium signalling regulates autophagy through calcineurin and TFEB. Nat Cell Biol 17, 288–299. [PubMed: 25720963]

Meijer WH, van der Klei IJ, Veenhuis M, and Kiel JA (2007). ATG genes involved in non-selective autophagy are conserved from yeast to man, but the selective Cvt and pexophagy pathways also require organism-specific genes. Autophagy 3, 106–116. [PubMed: 17204848]

Mizushima N, Noda T, Yoshimori T, Tanaka Y, Ishii T, George MD, Klionsky DJ, Ohsumi M, and Ohsumi Y (1998a). A protein conjugation system essential for autophagy. Nature 395, 395–398. [PubMed: 9759731]

Mizushima N, Sugita H, Yoshimori T, and Ohsumi Y (1998b). A new protein conjugation system in human. The counterpart of the yeast Apg12p conjugation system essential for autophagy. The Journal of biological chemistry 273, 33889–33892. [PubMed: 9852036]

Mizushima N, Yoshimori T, and Ohsumi Y (2011). The role of Atg proteins in autophagosome formation. Annu Rev Cell Dev Biol 27, 107–132. [PubMed: 21801009]

Morita E, Sandrin V, Chung HY, Morham SG, Gygi SP, Rodesch CK, and Sundquist WI (2007). Human ESCRT and ALIX proteins interact with proteins of the midbody and function in cytokinesis. EMBO J 26, 4215–4227. [PubMed: 17853893]

Nabhan JF, Hu R, Oh RS, Cohen SN, and Lu Q (2012). Formation and release of arrestin domain-containing protein 1-mediated microvesicles (ARMMs) at plasma membrane by recruitment of TSG101 protein. Proc Natl Acad Sci U S A 109, 4146–4151. [PubMed: 22315426]

Nabi IR, Shankar J, and Dennis JW (2015). The galectin lattice at a glance. J Cell Sci 128, 2213–2219. [PubMed: 26092931]

Napolitano G, and Ballabio A (2016). TFEB at a glance. Journal of Cell Science In press.

Nishimura T, Kaizuka T, Cadwell K, Sahani MH, Saitoh T, Akira S, Virgin HW, and Mizushima N (2013). FIP200 regulates targeting of Atg16L1 to the isolation membrane. EMBO Rep 14, 284–291. [PubMed: 23392225]

Noda T, and Ohsumi Y (1998). Tor, a phosphatidylinositol kinase homologue, controls autophagy in yeast. The Journal of biological chemistry 273, 3963–3966. [PubMed: 9461583]

North SJ, Huang HH, Sundaram S, Jang-Lee J, Etienne AT, Trollope A, Chalabi S, Dell A, Stanley P, and Haslam SM (2010). Glycomics profiling of Chinese hamster ovary cell glycosylation mutants reveals N-glycans of a novel size and complexity. The Journal of biological chemistry 285, 5759–5775. [PubMed: 19951948]

Olmos Y, Hodgson L, Mantell J, Verkade P, and Carlton JG (2015). ESCRT-III controls nuclear envelope reformation. Nature 522, 236–239. [PubMed: 26040713]

Pallikkuth S, Martin C, Farzam F, Edwards JS, Lakin MR, Lidke DS, and Lidke KA (2018). Sequential super-resolution imaging using DNA strand displacement. PLoS One 13, e0203291. [PubMed: 30169528]

Papadopoulos C, Kirchner P, Bug M, Grum D, Koerver L, Schulze N, Poehler R, Dressler A, Fengler S, Arhzaouy K, et al. (2017). VCP/p97 cooperates with YOD1, UBXD1 and PLAA to drive clearance of ruptured lysosomes by autophagy. EMBO J 36, 135–150. [PubMed: 27753622]

Park S, Buck MD, Desai C, Zhang X, Loginicheva E, Martinez J, Freeman ML, Saitoh T, Akira S, Guan JL, et al. (2016). Autophagy Genes Enhance Murine Gammaherpesvirus 68 Reactivation from Latency by Preventing Virus-Induced Systemic Inflammation. Cell Host Microbe 19, 91–101. [PubMed: 26764599]

Patnaik SK, Potvin B, Carlsson S, Sturm D, Leffler H, and Stanley P (2006). Complex N-glycans are the major ligands for galectin-1, -3, and -8 on Chinese hamster ovary cells. Glycobiology 16, 305–317. [PubMed: 16319083]

Patnaik SK, and Stanley P (2006). Lectin-resistant CHO glycosylation mutants. Methods Enzymol 416, 159–182. [PubMed: 17113866]

Petiot A, Ogier-Denis E, Blommaart EF, Meijer AJ, and Codogno P (2000). Distinct classes of phosphatidylinositol 3'-kinases are involved in signaling pathways that control macroautophagy in HT-29 cells. The Journal of biological chemistry 275, 992–998. [PubMed: 10625637]

Raab M, Gentili M, de Belly H, Thiam HR, Vargas P, Jimenez AJ, Lautenschlaeger F, Voituriez R, Lennon-Dumenil AM, Manel N, et al. (2016). ESCRT III repairs nuclear envelope ruptures during cell migration to limit DNA damage and cell death. Science 352, 359–362. [PubMed: 27013426]

Radulovic M, Schink KO, Wenzel EM, Nahse V, Bongiovanni A, Lafont F, and Stenmark H (2018). ESCRT-mediated lysosome repair precedes lysophagy and promotes cell survival. EMBO J 37.

Randow F, and Youle RJ (2014). Self and nonself: how autophagy targets mitochondria and bacteria. Cell Host Microbe 15, 403–411. [PubMed: 24721569]

Roczniak-Ferguson A, Petit CS, Froehlich F, Qian S, Ky J, Angarola B, Walther TC, and Ferguson SM (2012). The transcription factor TFEB links mTORC1 signaling to transcriptional control of lysosome homeostasis. Sci Signal 5, ra42. [PubMed: 22692423]

Ruhl S, Shkarina K, Demarco B, Heilig R, Santos JC, and Broz P (2018). ESCRT-dependent membrane repair negatively regulates pyroptosis downstream of GSDMD activation. Science 362, 956–960. [PubMed: 30467171]

Rusten TE, and Stenmark H (2009). How do ESCRT proteins control autophagy? J Cell Sci 122, 2179–2183. [PubMed: 19535733]

Saxton RA, and Sabatini DM (2017). mTOR Signaling in Growth, Metabolism, and Disease. Cell 168, 960–976. [PubMed: 28283069]

Scheffer LL, Sreetama SC, Sharma N, Medikayala S, Brown KJ, Defour A, and Jaiswal JK (2014). Mechanism of Ca(2)(+)-triggered ESCRT assembly and regulation of cell membrane repair. Nature communications 5, 5646.

Scott RC, Schuldiner O, and Neufeld TP (2004). Role and regulation of starvation-induced autophagy in the Drosophila fat body. Dev Cell 7, 167–178. [PubMed: 15296714]

Searle BC, Pino LK, Egertson JD, Ting YS, Lawrence RT, MacLean BX, Villen J, and MacCoss MJ (2018). Chromatogram libraries improve peptide detection and quantification by data independent acquisition mass spectrometry. Nature communications 9, 5128.

Settembre C, Di Malta C, Polito VA, Garcia Arencibia M, Vetrini F, Erdin S, Erdin SU, Huynh T, Medina D, Colella P, et al. (2011). TFEB links autophagy to lysosomal biogenesis. Science 332, 1429–1433. [PubMed: 21617040]

Settembre C, Zoncu R, Medina DL, Vetrini F, Erdin S, Huynh T, Ferron M, Karsenty G, Vellard MC, Facchinetti V, et al. (2012). A lysosome-to-nucleus signalling mechanism senses and regulates the lysosome via mTOR and TFEB. The EMBO journal 31, 1095–1108. [PubMed: 22343943]

Skowyra ML, Schlesinger PH, Naismith TV, and Hanson PI (2018). Triggered recruitment of ESCRT machinery promotes endolysosomal repair. Science 360.

Smith CS, Joseph N, Rieger B, and Lidke KA (2010). Fast, single-molecule localization that achieves theoretically minimum uncertainty. Nat Methods 7, 373–375. [PubMed: 20364146]

Stewart SE, Menzies SA, Popa SJ, Savinykh N, Petrunkina Harrison A, Lehner PJ, and Moreau K (2017). A genome-wide CRISPR screen reconciles the role of N-linked glycosylation in galectin-3 transport to the cell surface. J Cell Sci 130, 3234–3247. [PubMed: 28775154]

Stolz A, Ernst A, and Dikic I (2014). Cargo recognition and trafficking in selective autophagy. Nat Cell Biol 16, 495–501. [PubMed: 24875736]

Takahashi Y, He H, Tang Z, Hattori T, Liu Y, Young MM, Serfass JM, Chen L, Gebru M, Chen C, et al. (2018). An autophagy assay reveals the ESCRT-III component CHMP2A as a regulator of phagophore closure. Nature communications 9, 2855.

Thiele DL, and Lipsky PE (1990). Mechanism of L-leucyl-L-leucine methyl ester-mediated killing of cytotoxic lymphocytes: dependence on a lysosomal thiol protease, dipeptidyl peptidase I, that is enriched in these cells. Proc Natl Acad Sci U S A 87, 83–87. [PubMed: 2296607]

Thurston TL, Wandel MP, von Muhlinen N, Foeglein A, and Randow F (2012). Galectin 8 targets damaged vesicles for autophagy to defend cells against bacterial invasion. Nature 482, 414–418. [PubMed: 22246324]

Valley CC, Liu S, Lidke DS, and Lidke KA (2015). Sequential superresolution imaging of multiple targets using a single fluorophore. PLoS One 10, e0123941. [PubMed: 25860558]

van Niel G, Charrin S, Simoes S, Romao M, Rochin L, Saftig P, Marks MS, Rubinstein E, and Raposo G (2011). The tetraspanin CD63 regulates ESCRT-independent and -dependent endosomal sorting during melanogenesis. Dev Cell 21, 708–721. [PubMed: 21962903]

Vasta GR, Feng C, Gonzalez-Montalban N, Mancini J, Yang L, Abernathy K, Frost G, and Palm C (2017). Functions of galectins as 'self/non-self'-recognition and effector factors. Pathog Dis 75.

Velikkakath AK, Nishimura T, Oita E, Ishihara N, and Mizushima N (2012). Mammalian Atg2 proteins are essential for autophagosome formation and important for regulation of size and distribution of lipid droplets. Molecular biology of the cell 23, 896–909. [PubMed: 22219374]

Vietri M, Schink KO, Campsteijn C, Wegner CS, Schultz SW, Christ L, Thoresen SB, Brech A, Raiborg C, and Stenmark H (2015). Spastin and ESCRT-III coordinate mitotic spindle disassembly and nuclear envelope sealing. Nature 522, 231–235. [PubMed: 26040712]

Wang SF, Tsao CH, Lin YT, Hsu DK, Chiang ML, Lo CH, Chien FC, Chen P, Arthur Chen YM, Chen HY, et al. (2014). Galectin-3 promotes HIV-1 budding via association with Alix and Gag p6. Glycobiology 24, 1022–1035. [PubMed: 24996823]

Watson RO, Manzanillo PS, and Cox JS (2012). Extracellular M. tuberculosis DNA Targets Bacteria for Autophagy by Activating the Host DNA-Sensing Pathway. Cell 150, 803–815. [PubMed: 22901810]

Webster BM, Colombi P, Jager J, and Lusk CP (2014). Surveillance of nuclear pore complex assembly by ESCRT-III/Vps4. Cell 159, 388–401. [PubMed: 25303532]

Wei Y, Chiang WC, Sumpter R Jr., Mishra P, and Levine B (2017). Prohibitin 2 Is an Inner Mitochondrial Membrane Mitophagy Receptor. Cell 168, 224–238 e210. [PubMed: 28017329]

Yoshida Y, Yasuda S, Fujita T, Hamasaki M, Murakami A, Kawawaki J, Iwai K, Saeki Y, Yoshimori T, Matsuda N, et al. (2017). Ubiquitination of exposed glycoproteins by SCF(FBXO27) directs damaged lysosomes for autophagy. Proc Natl Acad Sci U S A 114, 8574–8579. [PubMed: 28743755]

Young AR, Chan EY, Hu XW, Kochl R, Crawshaw SG, High S, Hailey DW, Lippincott-Schwartz J, and Tooze SA (2006). Starvation and ULK1-dependent cycling of mammalian Atg9 between the TGN and endosomes. J Cell Sci 119, 3888–3900. [PubMed: 16940348]

HIGHLIGHTS

- A system for membrane repair, removal and replacement is coordinated by galectins
- Galectin-3 recruits ESCRT components to damaged lysosomes to repair them
- Galectins induce autophagy to remove damaged lysosomes and activate their biogenesis
- This galectin-directed system protects against *M. tuberculosis* and neurotoxic tau

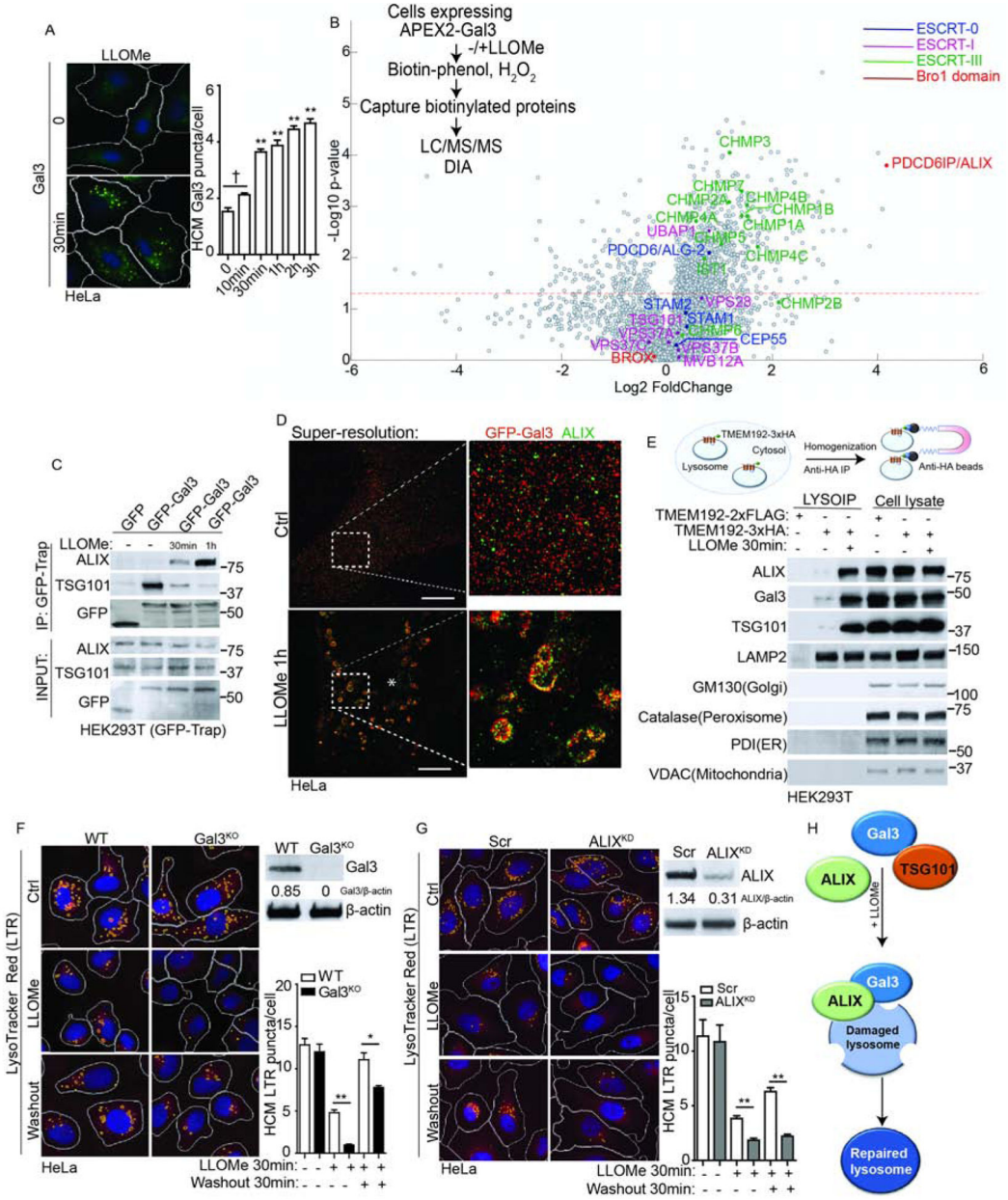

Figure 1. Galectin-3 and ESCRT component ALIX interact and protect lysosomes from damage.

(A) Time-response of Gal3 during lysosomal damage. HeLa cells were treated with 1mM LLOMe and endogenous Gal3 puncta quantified by high content microscopy (HCM). White masks, algorithm-defined cell boundaries (primary objects); Yellow masks, computer-identified Gal3 puncta (target objects). **(B)** EncyclopeDIA/scaffoldDIA analysis of Gal3 binding partners proximity-biotinylated by APEX2-Gal3 during lysosomal damage with 1mM LLOMe for 1h. Scatter (volcano) plot shows log2 fold change and −log10 *P* value for the proteins identified and quantified (LC/MS/MS) in 3 independent experiments (see Table S1, Tabs1 and 2). **(C)** Co-IP analysis of interactions between Gal3 and ALIX/TSG101 during lysosomal damage. **(D)** Superresolution microscopy analysis of ALIX and Gal3. HeLa cells transiently expressing GFP-Gal3 were treated with 1mM LLOMe for 1h. Scale

bar, 5 μm. **(E)** Analysis of lysosomes purified by anti-HA immunoprecipitation (LysoIP; TMEM192-3xHA) from HEK293T cells treated with 1mM LLOMe for 30min. TMEM192-2xFLAG, control. **(F)** Status of acidified organelles in parental HeLa (WT) and Gal3-KO HeLa cells ($Gal3^{KO}$) assessed by LysoTracker HCM during lysosomal damage (1mM LLOMe for 30min followed by 30min washout). Ctrl, control (untreated cells). Yellow masks, computer-identified LTR puncta. **(G)** As in F, ALIX knockdown ($ALIX^{KD}$). Scr, scrambled siRNA. **(H)** Schematic summary of the findings in Figure 1. Data, means ± SEM; HCM: $n \geq 3$ (each experiment: 500 valid primary objects/cells per well, ≥ 5 wells/sample). † $p \geq 0.05$ (not significant), *$p < 0.05$, **$p < 0.01$, ANOVA. See also Figure S1 and S2.

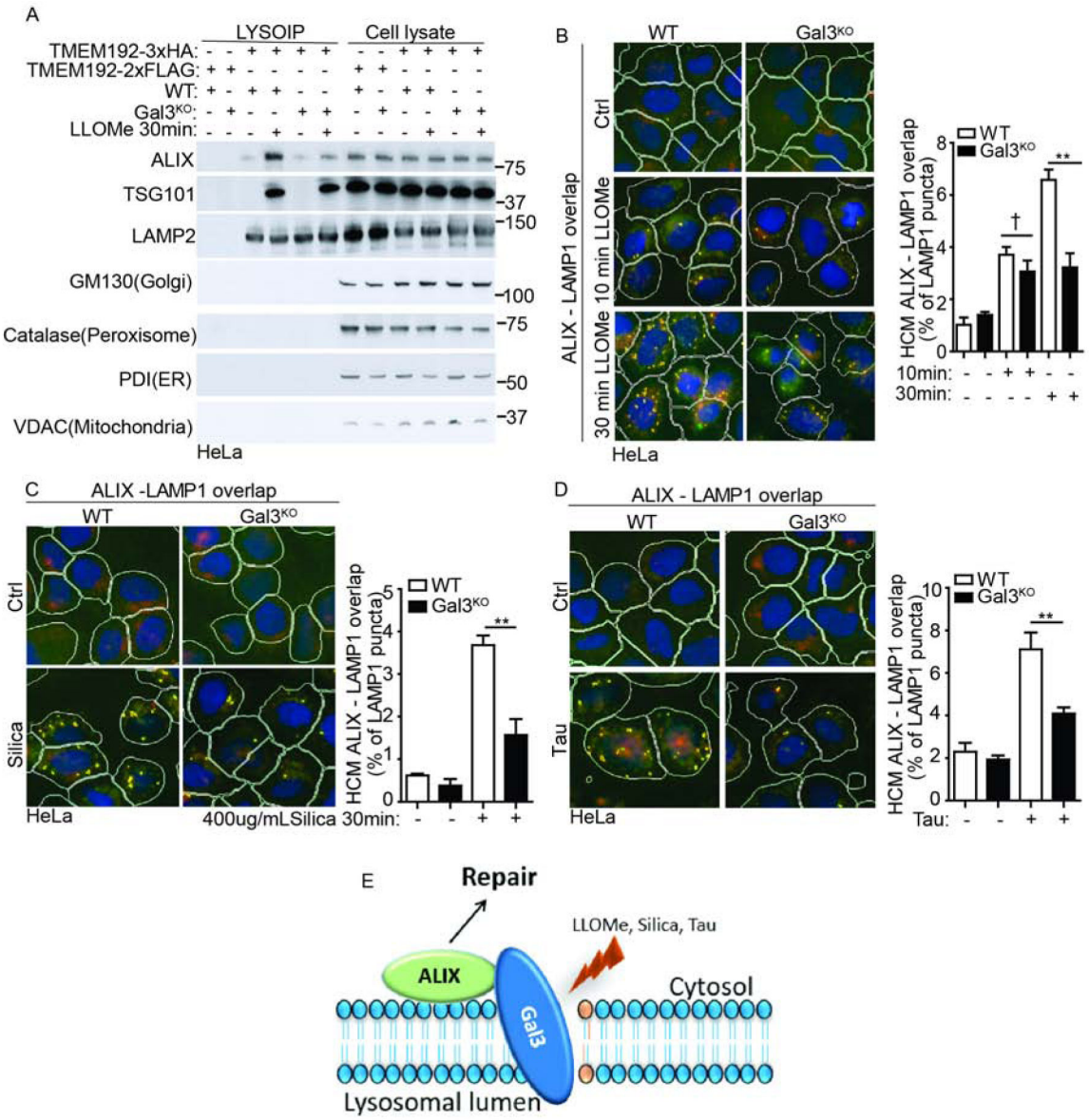

Figure 2. Galectin-3 is required for efficient recruitment of ALIX to damaged lysosomes.

(A) LysoIP analysis for indicated proteins in cell lysates or lysosomes purified from parental HeLa (WT) and Gal3-knockout HeLa cells (Gal3^{KO}) subjected to the 1mM LLOMe treatment for 30min. **(B)** Quantification by HCM of overlaps between ALIX and LAMP1 in parental HeLa (WT) and Gal3-knockout HeLa cells (Gal3^{KO}) during lysosomal damage. **(C)** Quantification by HCM of overlaps between ALIX and LAMP1 in parental HeLa (WT) and Gal3-knockout HeLa cells (Gal3^{KO}) during 400 μg/mL silica treatment. **(D)** Quantification by HCM of overlaps between ALIX and LAMP1 in parental HeLa (WT) and Gal3-knockout HeLa cells (Gal3^{KO}) during Tau oligomer treatment. Cells were treated with 1μg/mL Tau oligomer overnight and subjected to HCM analysis. **(E)** Schematic summary of the findings in Figure 2. None-treated cells were used as control (Ctrl). White masks, algorithm defined cell boundaries; Yellow masks, computer-identified overlap of ALIX and LAMP1. See also Figure S2.

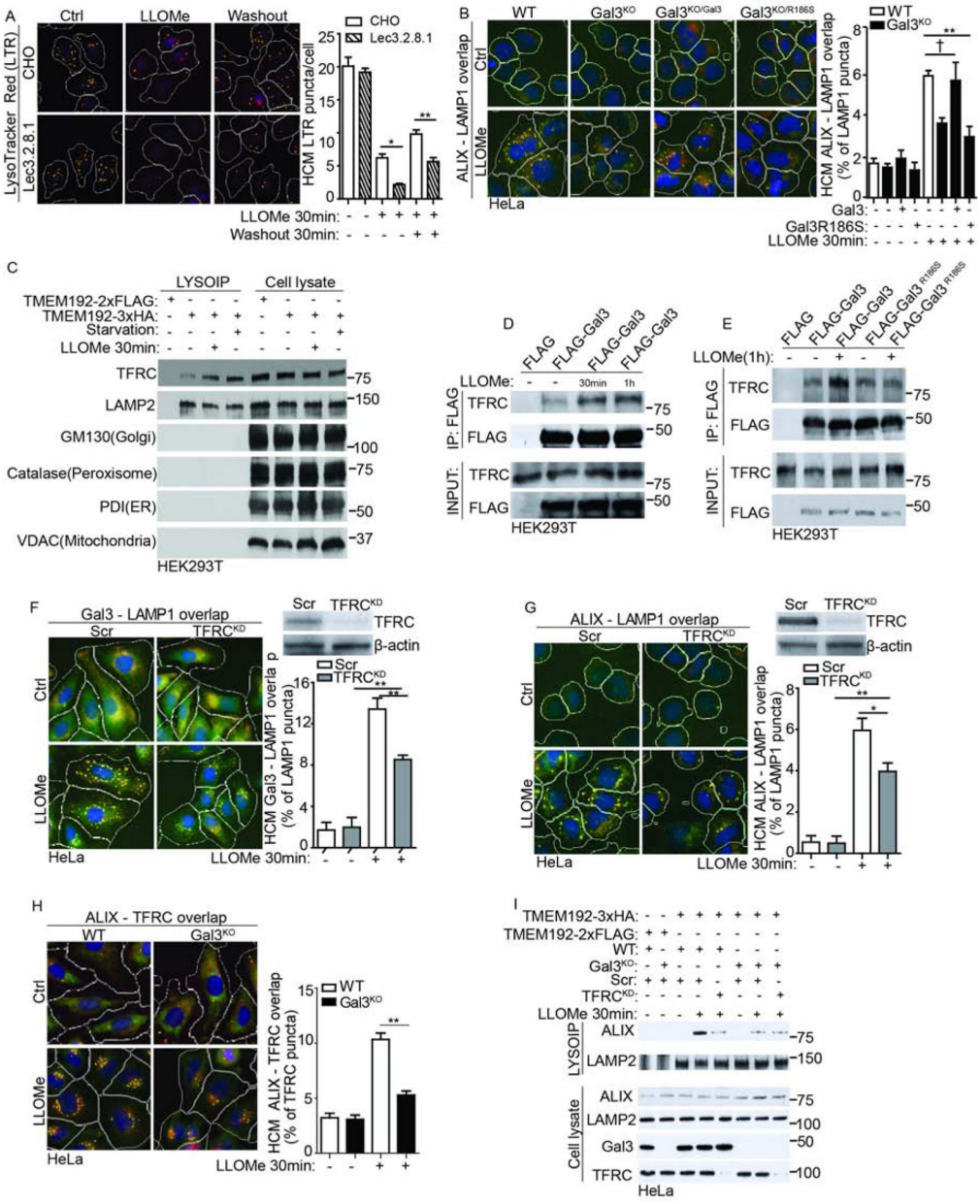

Figure 3. Glycosylation and specific glycosylated proteins play a role in Gal3 recognition of lysosomal damage.

(A) HCM Analysis of the status of acidified organelles in wild-type CHO cells and mutant Lec3.2.8.1 by LysoTracker during lysosomal damage. As in Fig. 1F. **(B)** Quantification by HCM of overlaps between ALIX and LAMP1 in parental HeLa (WT) and Gal3-knockout HeLa cells (Gal3^{KO}). As in Fig. 2B. **(C)** LysoIP analysis for indicated proteins in cell lysates or lysosomes purified from parental HeLa cells subjected to 1mM LLOMe or starvation (EBSS medium) treatment for 30min. **(D)** Co-immunoprecipitation analysis of changes in interactions between Gal3 and TFRC during the process of lysosomal damage. **(E)** Co-immunoprecipitation analysis of changes in interactions between Gal3/Gal3^{R186S} and TFRC during the process of lysosomal damage. **(F)** Quantification by HCM of overlaps between

Gal3 and LAMP1 in parental HeLa (WT) and TFRC-knockdown HeLa cells ($TFRC^{KD}$) during LLOMe treatment. **(G)** Quantification by HCM of overlaps between ALIX and LAMP1 in parental HeLa (WT) and TFRC-knockdown HeLa cells ($TFRC^{KD}$) during LLOMe treatment. **(H)** Quantification by HCM of overlaps between ALIX and TFRC in parental HeLa (WT) and Gal3-knockout HeLa cells ($Gal3^{KO}$) during LLOMe treatment. **(I)** LysoIP analysis for indicated proteins in cell lysates or lysosomes purified from parental HeLa (WT) and Gal3-knockout HeLa cells ($Gal3^{KO}$) with or without TFRC-knockdown ($TFRC^{KD}$). None-treated cells were used as control (Ctrl). White masks, algorithm defined cell boundaries; Yellow masks, computer-identified overlap of two proteins. See also Figure S3.

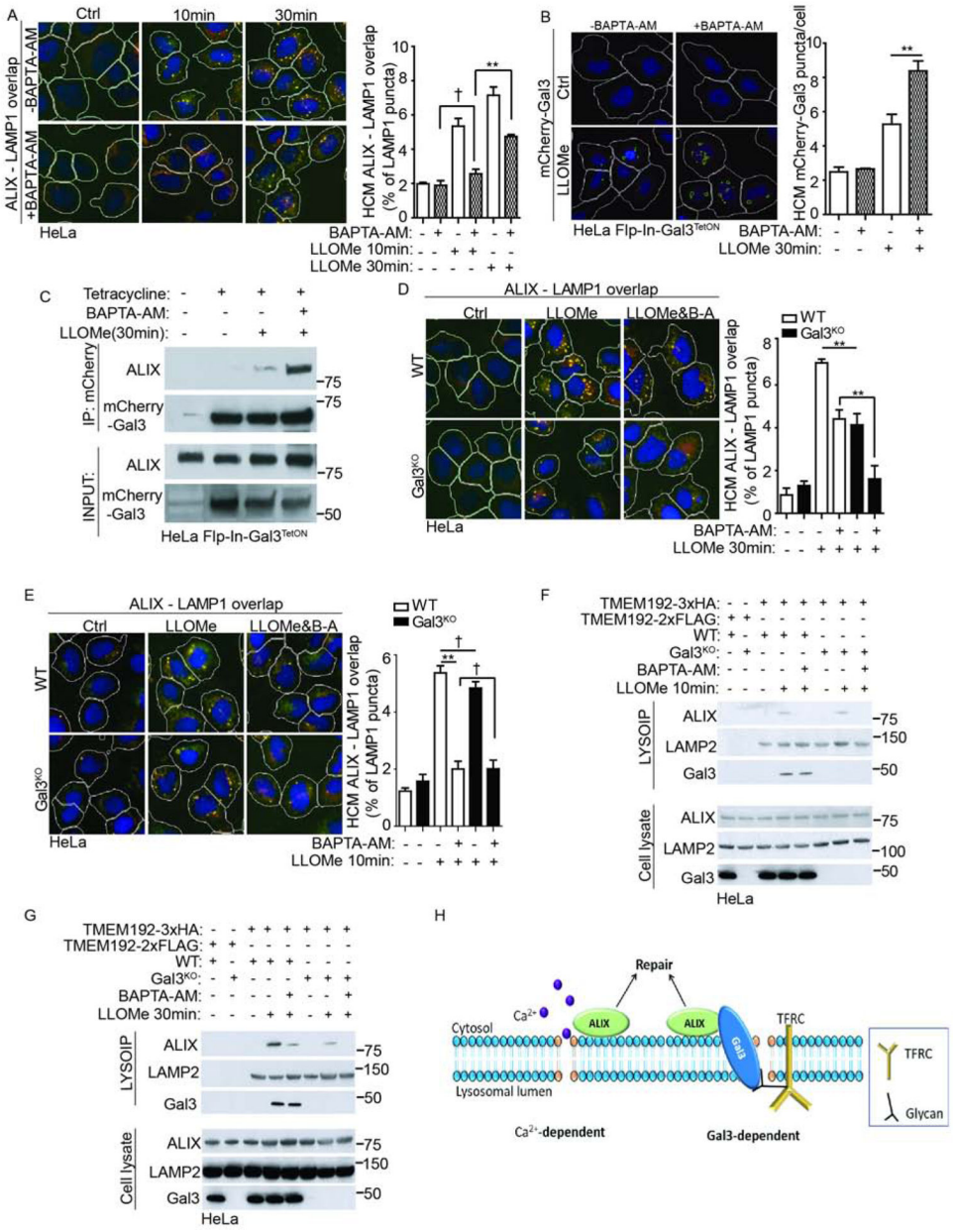

Figure 4. Optimal ALIX recruitment to damaged lysosomes requires two signals.

(A) Cells were treated with 15μM BAPTA-AM for 1h, subjected to 1mM LLOMe treatment for the indicated time, followed by HCM analysis of overlaps between ALIX and LAMP1. As in Fig. 2B. **(B)** The constructed HeLa Flp-In-Gal3^{TetON} cells stably expressing mCherry-Gal3 induced by tetracycline were subject to 15μM BAPTA-AM treatment for 1h and then treated with LLOMe. **(C)** Co-immunoprecipitation analysis of changes in interactions between Gal3 and ALIX under BAPTA-AM treatment during lysosomal damage. **(D)** Quantification by HCM of overlaps between ALIX and LAMP1 in parental HeLa (WT) and Gal3-knockout HeLa cells (Gal3^{KO}) treated with BAPTA-AM during lysosomal damage. **(E)** Quantification by HCM of overlaps between ALIX and LAMP1 in parental HeLa (WT) and Gal3-knockout HeLa cells (Gal3^{KO}) treated with BAPTA-AM during lysosomal

damage. **(F)** LysoIP analysis for indicated proteins in cell lysates or lysosomes purified from parental HeLa (WT) and Gal3-knockout HeLa cells ($Gal3^{KO}$) treated with 15μM BAPTA-AM for 1h subjected to the 1mM LLOMe treatment for 10min. **(G)** LysoIP analysis for indicated proteins in cell lysates or lysosomes purified from parental HeLa (WT) and Gal3-knockout HeLa cells ($Gal3^{KO}$) treated with 15μM BAPTA-AM for 1h subjected to LLOMe treatment. **(H)** Schematic summary of the findings in Figure 4.

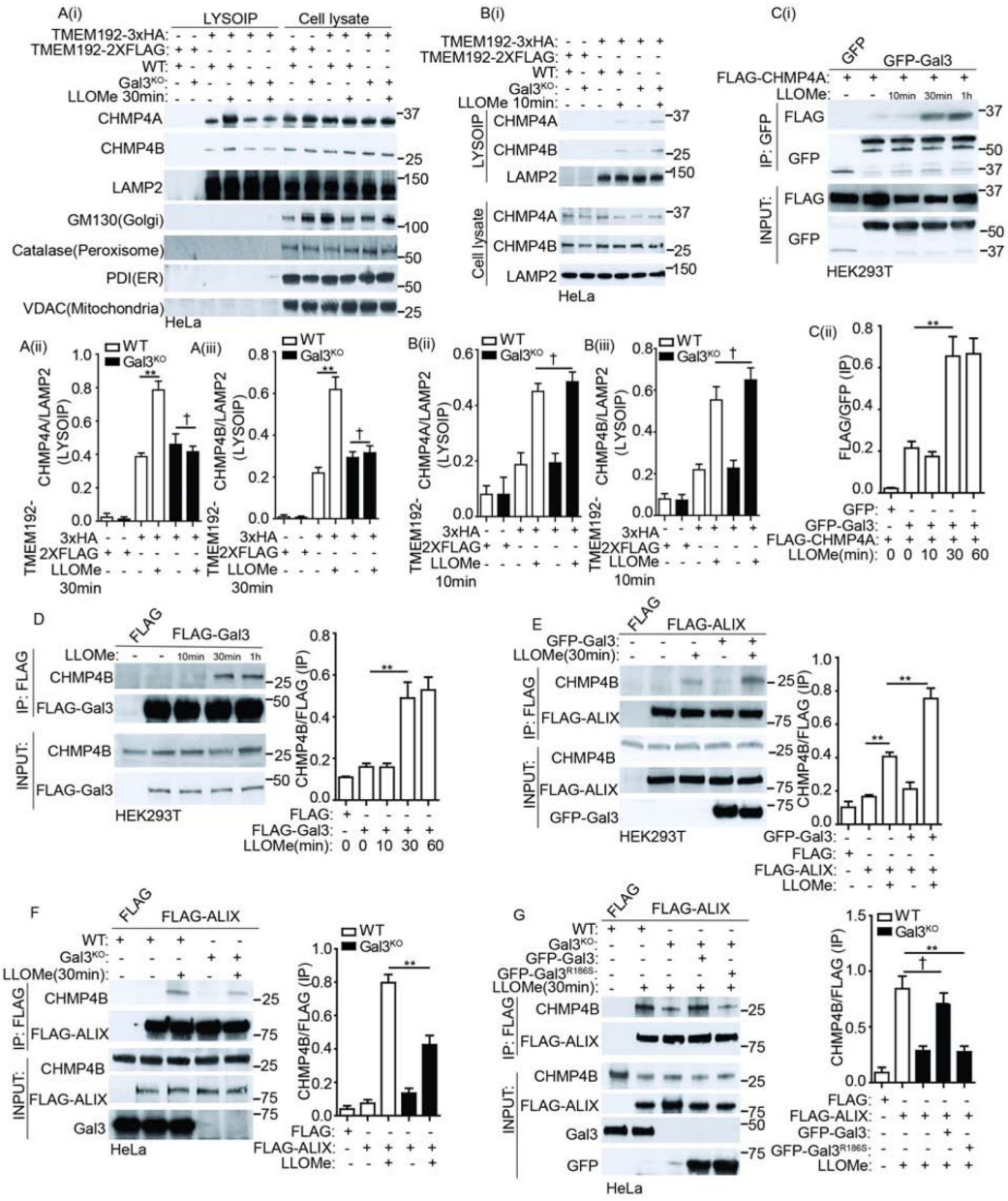

Figure 5. Galectin-3 promotes response of core ESCRT-III effectors during lysosomal damage.

(A)(i) LysoIP analysis for indicated proteins in cell lysates or lysosomes purified from parental HeLa (WT) and Gal3-knockout HeLa cells (Gal3^{KO}) after 1mM LLOMe treatment for 30min. (ii-iii) Quantification of LysoIP analysis for CHMP4A and CHMP4B. **(B)**(i) LysoIP analysis for indicated proteins in cell lysates or lysosomes purified from parental HeLa (WT) and Gal3-knockout HeLa cells (Gal3^{KO}) after 1mM LLOMe treatment for 10min. (ii-iii) Quantification of LysoIP analysis for CHMP4A and CHMP4B. **(C)** Co-immunoprecipitation analysis of changes in interactions between Gal3 and CHMP4A during the process of lysosomal damage. **(D)** Co-immunoprecipitation analysis of changes in interactions between Gal3 and CHMP4B during the process of lysosomal damage. **(E)** Co-immunoprecipitation analysis of the effect of Gal3 on the interaction between ALIX and

CHMP4B during lysosomal damage. **(F)** Co-immunoprecipitation analysis of the interaction between ALIX and CHMP4B in parental HeLa (WT) and Gal3-knockout HeLa cells ($Gal3^{KO}$) during lysosomal damage. **(G)** Co-immunoprecipitation analysis of the effect of Gal3 and its mutant $Gal3^{R186S}$ on the interaction between ALIX and CHMP4B. See also Figure S5.

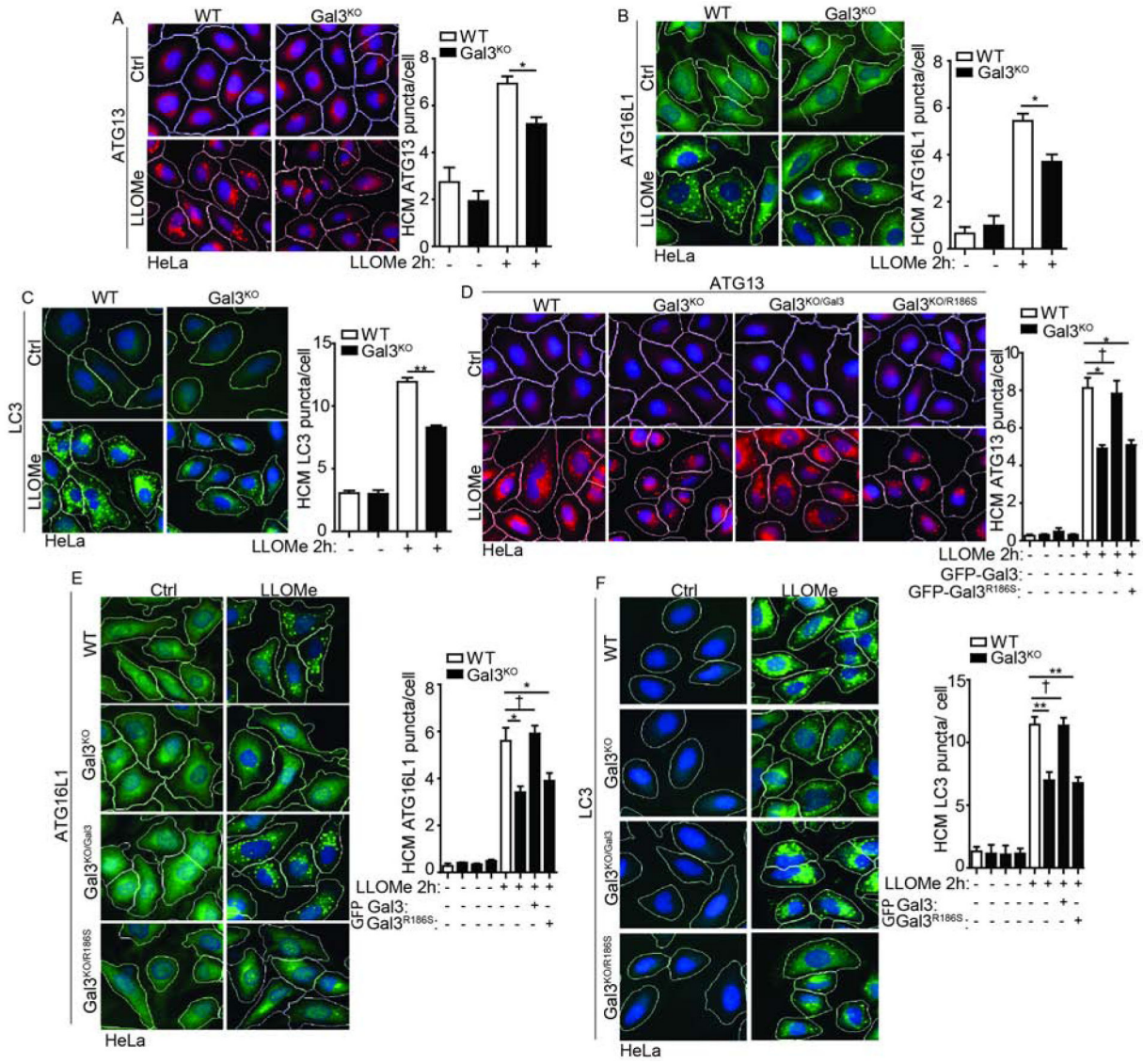

Figure 6. Galectin-3 is important for autophagy response to lysosomal damage.

(A) HeLa cells were treated with 1mM LLOMe for 2h and subjected to HCM analysis of ATG13 puncta. **(B)** HeLa cells were treated with 1mM LLOMe for 2h and subjected to HCM analysis of ATG16L1 puncta. **(C)** HeLa cells were treated with 1mM LLOMe for 2h and subjected to HCM analysis of LC3. **(D)** Gal3-knockout HeLa cells ($Gal3^{KO}$) transfected with GFP-tagged WT Gal3 or $Gal3^{R186S}$ were treated with 1mM LLOMe for 2h and subjected to HCM analysis of ATG13 puncta. **(E)** Gal3-knockout HeLa cells ($Gal3^{KO}$) transfected with GFP-tagged WT Gal3 or $Gal3^{R186S}$ were treated with 1mM LLOMe for 2h and subjected to HCM analysis of ATG16L1 puncta. **(F)** Gal3-knockout HeLa cells ($Gal3^{KO}$) transfected with GFP-tagged WT Gal3 or -$Gal3^{R186S}$ were treated with 1mM LLOMe for 2h and the puncta of LC3 was quantified using HCM. None-treated cells were used as control (Ctrl). White masks, algorithm defined cell boundaries; Red masks, computer-identified target protein puncta. See also Figure S5.

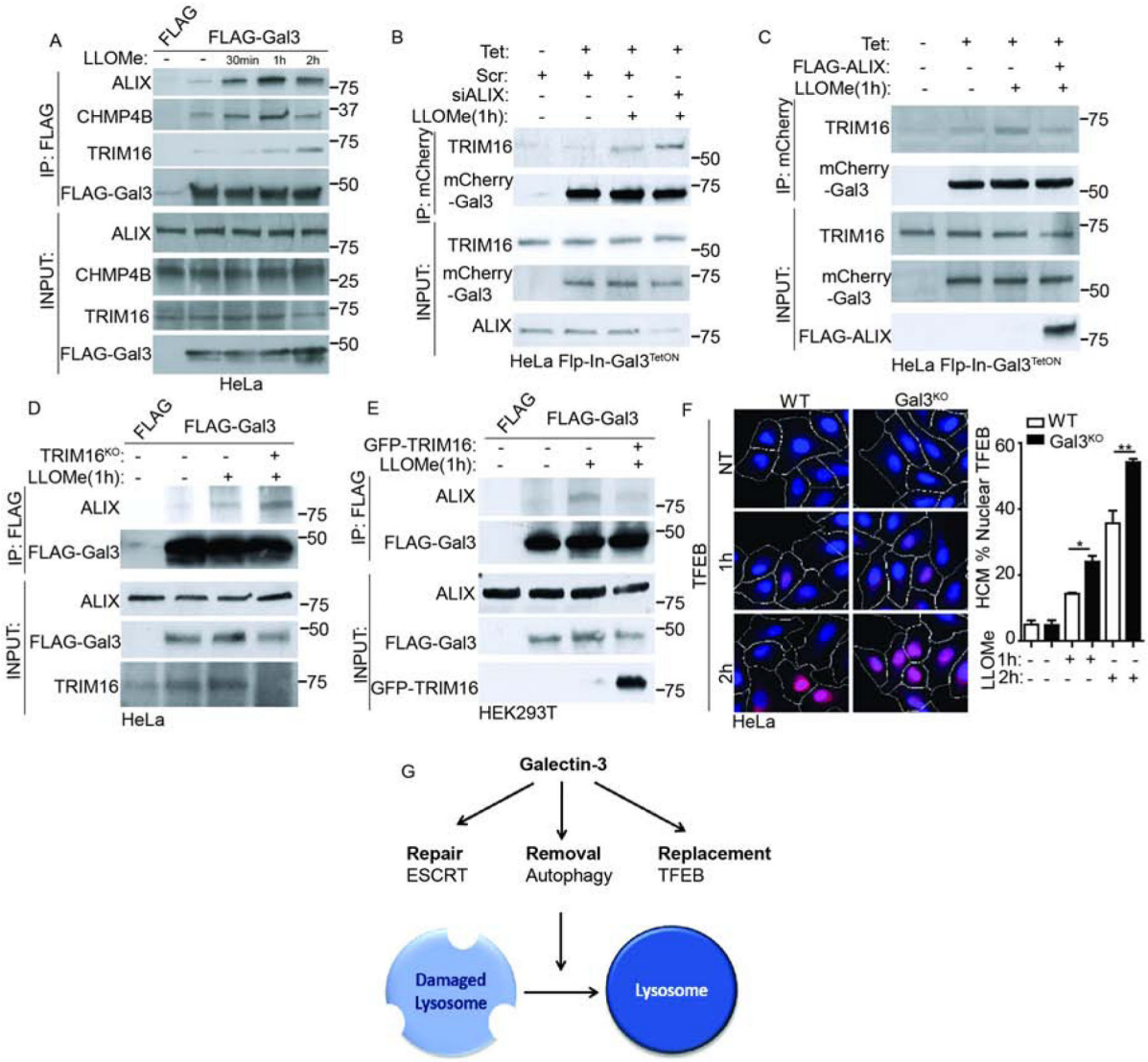

Figure 7. Galectin-3 serves as a switch between ESCRT and autophagy responses to lysosomal damage.

(A) Co-immunoprecipitation analysis of changes in interactions between Gal3 and ESCRT components during the process of lysosomal damage. **(B)** The constructed HeLa Flp-In-Gal3^{TetON} cells stably expressing Gal3 induced by tetracycline (Tet) were subject to ALIX knockdown and then treated with 1mM LLOMe for 1h. **(C)** Co-immunoprecipitation analysis of the effect of ALIX on interaction between Gal3 and TRIM16 during lysosomal damage. **(D)** Co-immunoprecipitation analysis of the effect of TRIM16 on the interaction between ALIX and Gal3 during lysosomal damage. **(E)** Co-immunoprecipitation analysis of the effect of TRIM16 on interaction between Gal3 and ALIX during lysosomal damage. **(F)** TFEB nuclear translocation in parental HeLa (WT) and Gal3-knockout HeLa cells (Gal3^{KO}) during lysosomal damage. Blue: nuclei, Hoechst 33342; Red: anti-TFEB antibody, Alexa-568. White masks, computer algorithm-defined cell boundaries; Pink masks,

computer-identified nuclear TFEB based on the average intensity of Alexa-568 fluorescence. **(G)** Schematic summary of the findings in Figure 7. See also Figure S6.

KEY RESOURCES TABLE

REAGENT or RESOURCE	SOURCE	IDENTIFIER
Antibodies		
Rabbit Anti-Galectin-3	Abcam	ab53082
Rabbit Anti-GFP	Abcam	ab290
Rabbit Anti-GFP(6AT316)	Abcam	ab38689
Rabbit Anti-mCherry	Abcam	ab183628
Rabbit Anti-VDAC1/Porin	Abcam	ab15895
Rabbit Anti-CHMP4B	Abcam	ab105767
Mouse Anti-CHMP4A	Abcam	ab67058
Mouse Anti-GM130	Abcam	ab1299
Mouse Anti-P4HB(PDI) (RL90)	Abcam	ab2792
Mouse Anti-TSG101(4A10)	Abcam	ab83
Rabbit Anti-LC3	MBL International	PM036
Rabbit Anti-ATG16L1	MBL International	PM040
Mouse Anti-Galectin-3	BioLegend	#125402
Mouse Anti-ALIX	BioLegend	#634502
Rabbit TFEB	Cell Signaling Technology	#4240
Rabbit ATG13(E1Y9V)	Cell Signaling Technology	#13468
Rabbit LAMP1(D2D11)	Cell Signaling Technology	#9091
Mouse Anti-FLAG M2	Sigma Aldrich	F1804
Mouse Anti-Transferrin Receptor	ThermoFisher	#13-6800
Clean-Blot IP Detection Kit (HRP)	ThermoFisher	21232
Alexa Fluor 488 secondary antibody	ThermoFisher	A-11029
Alexa Fluor 568 secondary antibody	ThermoFisher	A-11036
Mouse LAMP2	DSHB of University of Iowa	H4B4
Rabbit Anti-TRIM16	Bethyl	A301-160A
Mouse Myc (9E10)	Santa Cruz Biotechnology	sc-40
Rabbit beta-Actin (C4)	Santa Cruz Biotechnology	sc-47778
Rabbit Galectin-8(H-80)	Santa Cruz Biotechnology	sc-28254
Goat anti-rabbit IgG-HRP secondary antibody	Santa Cruz Biotechnology	sc-2004
Goat anti-mouse IgG-HRP secondary antibody	Santa Cruz Biotechnology	sc-2005
Bacterial and Virus Strains		
NEB 5-alpha Competent *E.coli* (High Efficiency)	New England Biolabs	C2987
One Shot Mach1 Phage-Resistant Competent *E.coli*	ThermoFisher	C862003
Mycobacterium tuberculosis Erdman	(Martina et al., 2012)	N/A
Mycobacterium tuberculosis ESX-1 mutant	(Martina et al., 2012)	N/A
Chemicals, Peptides, and Recombinant Proteins		
Leu-Leu-methyl ester hydrobromide (LLOMe)	Sigma Aldrich	L7393

REAGENT or RESOURCE	SOURCE	IDENTIFIER
Gly-Phe-beta-Naphthylamide (GPN)	Cayman Chemicals	21438-66-4
Biotinyl tyramide (biotin-phenol)	AdipoGen LIFE SCIENCES	CDX-B0270-M100
sodium ascorbate	Sigma Aldrich	A7631
sodium azide	Sigma Aldrich	S2002
Trolox	Sigma Aldrich	238813
BAPTA-AM	Sigma Aldrich	A1076
Tetracycline hydrochloride	Sigma Aldrich	T3383
Puromycin dihydrochloride	Sigma Aldrich	P9620
Silica crystal	US Silica	MIN-U-SIL-15
mouse macrophage colony stimulating factor (mM-CSF)	Cell Signaling Technology	5228
Hoechst 33342	ThermoFisher	H3570
Prolong Gold Antifade Mountant with DAPI	ThermoFisher	P36931
LysoTracker Red DND-99	ThermoFisher	L7528
LysoTracker Green DND-26	ThermoFisher	L7526
LR Clonase II Plus Enzyme Mix	ThermoFisher	11791100
BP Clonase II Plus Enzyme Mix	ThermoFisher	11789100
Critical Commercial Assays		
ProFection Mammalian Transfection System	Promega	E1200
Amaxa Cell Line Nucleofector Kit R	Lonza	VCA-1001
Lipofectamine RNAiMAX Transfection Reagent	ThermoFisher	13778030
Lipofectamine 2000 Transfection Reagent	ThermoFisher	12566014
Magic Red Cathepsin-B Assay	ImmunoChemistry	#938
Deposited Data		
Raw MS DIA/DDA data	https://massive.ucsd.edu	MSV000083998
Raw MS DIA/DDA data	http://www.proteomexchange.org	ProteomeXchange: PXD014304
Original microscopy and western blots	This paper; Mendeley data	http://dx.doi.org/10.17632/v52k86mp58.1
Experimental Models: Cell Lines		
HeLa Flp-In-Gal3^{TetON}	This study	N/A
HEK293T-TMEM192-2XFLAG	This study	N/A
HEK293T-TMEM192-3XHA	This study	N/A
HeLa-TMEM192-2XFLAG	This study	N/A
HeLa-TMEM192-3XHA	This study	N/A
Gal3^{KO}-TMEM192-2XFLAG	This study	N/A
Gal3^{KO}-TMEM192-3XHA	This study	N/A
Huh7 Gal9^{KO}	This study	N/A
HeLa Gal3^{KO}	(Jia et al., 2018)	N/A
HeLa Gal8^{KO}	(Jia et al., 2018)	N/A

REAGENT or RESOURCE	SOURCE	IDENTIFIER
HeLa TRIM16^{KO}	(Chauhan et al., 2016)	N/A
CHO/ Lec3.2.8.1	Dr. Stanley (Patnaik et al., 2006)	N/A
Experimental Models: Organisms/Strains		
LysM-Cre TRIM16$^{fl/fl}$ mice derivative in C57/BL6 background Genotyping service provided by Transnetyx	This study	N/A
Oligonucleotides		
Gal3^{R186S}-mutant oligonucleotide sense 5'-ATGGGAAAACCGACTGGCTTTCTTCCCTTCCCC-3'	Integrated DNA Technologies	N/A
Gal3^{R186S}-mutant oligonucleotide anti-sense 5'-GGGGAAGGGAAGAAAGCCAGTCGGTTTTCCCA-3'	Integrated DNA Technologies	N/A
Gal3^{PSAP}-mutant oligonucleotide sense 5'-GGTAGGCTCCGGGGGCACTTGGCTG-3'	Integrated DNA Technologies	N/A
Gal3^{PSAP}-mutant oligonucleotide anti-sense 5'-CAGCCAAGTGCCCCCGGAGCCTACC-3'	Integrated DNA Technologies	N/A
ALIX-Gateway oligonucleotide sense 5'-GGGGACAAGTTTGTACAAAAAAGCAGGCTTCGCGACATTCATCTCGGTGCAGCTG-3'	Integrated DNA Technologies	N/A
ALIX-Gateway oligonucleotide anti-sense 5'-GGGGACCACTTTGTACAAGAAAGCTGGGTCTTACTGCTGTGGATAGTAAGACTG-3'	Integrated DNA Technologies	N/A
CHMP4A-Gateway oligonucleotide sense 5'-GGGGACAAGTTTGTACAAAAAAGCAGGCTTCTCGCGGCGGCGCCCTGAGGACG-3'	Integrated DNA Technologies	N/A
CHMP4A-Gateway oligonucleotide anti-sense 5'-GGGGACCACTTTGTACAAGAAAGCTGGGTCTCAGGATACCCACTCAGCCAAC-3'	Integrated DNA Technologies	N/A
The probe CRE of LysM-Cre TRIM16$^{fl/fl}$ Forward primer TTAATCCATATTGGCAGAACGAAAACG	Integrated DNA Technologies	N/A
The probe CRE of LysM-Cre TRIM16$^{fl/fl}$ Reverse primer CAGGCTAAGTGCCTTCTCTACA	Integrated DNA Technologies	N/A
SiGENOME human PDCD6IP(ALIX) siRNA (SMARTpool)	Dharmacon	M-004233-02-0005
SiGENOME human TFRC siRNA (SMARTpool)	Dharmacon	M-003941-02-0005
Recombinant DNA		
pCINeoFLAG ALIX	Addgene	#89859
pDONR223-CHMP4A	DNASU	HsCD00398951
pDONR221-TSG101	DNASU	HsCD00044844
pCAG.MCS2.C-Myc-CHMP4B	DNASU	HsCD00696231
pDEST-FLAG-Gal3^{PSAP}	This work	N/A
pDEST-FLAG-TSG101	This work	N/A
pDEST-GFP-TSG101	This work	N/A
pDEST-mCherry-TSG101	This work	N/A
pDEST-FLAG-Gal3^{R186S}	This work	N/A
pDEST-GFP- Gal3^{R186S}	This work	N/A
pDEST-FLAG-ALIX	This work	N/A
pDEST-mCherry-ALIX	This work	N/A
pDEST-FLAG-CHMP4A	This work	N/A

REAGENT or RESOURCE	SOURCE	IDENTIFIER
pDEST-mCherry-CHMP4A	This work	N/A
pDEST-Gal3(1-112)	This work	N/A
pDEST-Gal3(113-250)	This work	N/A
pGFP-LAMP1	This work	N/A
pLJC5-TMEM192-3xHA	Addgene	#102930
pLJC5-TMEM192-2xFLAG	Addgene	#102929
pCMV-VSV-G	Addgene	#8454
psPAX2	Addgene	#12260
pJJiaDEST-APEX2-Gal3	(Jia et al., 2018)	N/A
pDEST-GFP-Gal8	(Jia et al., 2018)	N/A
pDEST-GFP-Gal9	(Jia et al., 2018)	N/A
pDEST-FLAG-Gal3	(Chauhan et al., 2016)	N/A
pDEST-GFP-Gal3	(Chauhan et al., 2016)	N/A
pDEST-GFP-TRIM16	(Chauhan et al., 2016)	N/A
Software and Algorithms		
iDEV software	ThermoFisher	N/A
AIM software	Carl Zeiss	N/A
Scaffold software	Proteome Software Inc	N/A
MATLAB software	MathWorks	N/A
Other		
RIPA Lysis Buffer	ThermoFisher	89900
NP40 Cell Lysis Buffer	ThermoFisher	FNN0021
Protease Inhibitor Cocktail Tablets	Roche	11697498001
PMSF	Sigma Aldrich	93482
Anti-HA Magnetic Beads	ThermoFisher	88836
Dynabeads Protein G	ThermoFisher	10003D
Streptavidin Magnetic Beads	ThermoFisher	88816
GFP-Trap MA (Magnetic Beads)	Ychromotek	61122001MA